Study of surface effects induced by Quasi-atomic layer etching

Master's thesis

Author: Oscar Danielsson

Supervisors:

Amin Karimi, AlixLabs AB

Ivan Maximov, Lund University

Sabbir Ahmed Khan, Danish Fundamental Metrology

M.Sc.-project on ALE damage

31-06-2024

Contents

Theoretical background 8

2.2 Atomic layer etching 10

2.2.1 Activation (step 1) 11

2.2.2 Purging step (step 2) 12

2.2.3 Etching step (step 3) 12

2.2.4 Purging step (step 4) 16

2.3 Damage formation 17

2.3.1 Incomplete etching 17

2.3.2 Dangling bonds 18

2.3.3 Sputtering 19

Method 22

3.1 Experimental tools and conditions 22

3.1.1 Inductively coupled plasma-reactive ion etching 22

3.1.2 Retarding field energy analyser 26

3.1.3 Ellipsometry 28

3.1.4 Scanning electron microscope 30

3.1.5 Atomic force microscope 32

3.2 Protocol 34

3.2.1 RFEA measurements of Ar+ ion energy and flux 34

3.2.1 Sample preparation and ellipsometry setup 35

3.2.1 Reactive ion etching and ALE experiments 36

3.2.1 Surface damage evaluation by EDS and AFM 38

Result and Discussion 39

4.1 RFEA measurements of Ar+ ion energy and flux 39

4.2 Etch Per Cycle Analysis: Effects of Bias, Bombardment time, and number of Cycles 43

4.3 Ellipsometry Analysis of the Layers Thickness 48

4.4 Surface damage evaluation by EDS and AFM 50

Conclusions and further outlook 60

5.1 Conclusions 60

5.2 Further outlook 61

List of abbreviations

AFM *Atomic force microscope*

A.U. *Arbitrary units*

ALD *Atomic layer deposition*

Ar *Argon*

Ar+ *Argon positively charged ion*

BSE *Backscattered electrons*

Br *Bromine*

BOE *Buffered oxide etchant*

Br *Bromine*

BOE *Buffered oxide etchant*

C° *Degrees Celsius*

C *Carbon*

Cl *Chlorine*

Cl- *Chlorine negatively charged ion*

DC *Direct current*

DFT *Density function theory*

DI *Deionized water*

EDS *Energy dispersive spectroscopy*

eV *Electron volt*

EPC *Etch per cycle*

F *Fluorine*

H *Hydrogen*

HF *Hydro fluoric acid*

Hz *Hertz*

ICP *Inductively coupled plasma*

IEDF *Ion energy distribution function*

MD *Molecular dynamic*

MFC *Mass flow controller*

Min *Minute*

MSE *Mean square error*

mTorr *millitorr*

N *Nitrogen*

O *Oxygen*

PC *Personal computer*

RF *Radio frequency*

RFEA *Retarding field energy analyser*

RIE *Reactive ion etching*

Rq *Root mean square*

S *Seconds*

sccm *Standard cubic centimetre per minute*

SCU *Semion control unit*

SE *Secondary electrons*

SEM *Scanning electron microscopy*

Si *Silicon*

SOI *Silicon on insulator*

W *Watt*

Q-ALE *quasi-ALE*

Å *Ångström*

Abstract

Atomic Layer Etching (ALE) is a self-limiting cyclic dry etching process used in nanofabrication that allows for material etching on the atomic scale in a layer-by-layer regime. In practical applications, such as using commercially available reactive ion etching (RIE) tools, the ion energy in the plasma exceeds the sputtering threshold (typically 20 to 40 eV for Si), leading to a Quasi-ALE (Q-ALE) regime. In this regime, the process steps are not self-limiting, but they are still highly accurate and result in lower damage than RIE. Direct measurements of the ion energy in Q-ALE are thus instrumental in studies of the etching process and the effects of surface damage. In this project, we are trying to achieve damage-free Q-ALE etching that will improve surface roughness by analysing the behaviour of the Si etching process. A damage-free Q-ALE process should be avoided from all sorts of imperfections and altering of the physical, optical, and electronic properties of the material. The project used a commercial Inductively Coupled Plasma RIE tool from Plasma-Therm LLC, USA. The tool operates in a Cl_2-molecular activation regime using Ar RF plasma to desorb the etch reaction products in the etch step. Unpatterned silicon-on-insulator (SOI) 10x10 mm^2 samples with a 50 nm thick top Si layer were used for the etching experiments and characterised by spectroscopic ellipsometry and atomic force microscopy (AFM). The experiments were operated in a 25-cycle mode, which was sufficient to measure the Si thickness difference by ellipsometry using a 4-layer optical model. A retarding field energy analyser (RFEA) from Impedance LLC, Ireland, was installed to measure the Ar+ ion energy distribution function (IEDF) and ion flux at different Q-ALE conditions, such as RF-power and pressure, to understand the behaviour inside of the RIE to achieve damage-free Q-ALE etching. The etched SOI samples' surface composition, surface damage, and surface roughness were characterised by AFM, SEM, and EDS.

We present the actual data of Ar+ IEDF and the ion flux at the sample level in the commercial RIE tool operating in a Q-ALE mode. To reach a low ion energy regime, we used a DC bias setpoint in the range of 10-120 V bias voltage, which corresponds respectively to the ion energy of 50 to 147 eV on the surface of the substrate inside of the RIE, according to the IEDF peak shifts measurements by RFEA. In the same ion energy range, the ion flux was measured to be approximately $3x10^{13}$– $2x10^{14}$cm^{2}2s, which fits well with the published data of molecular dynamic simulations (MD) of similar processes under the same condition. Etch per cycle (EPC) was measured in both sputtering (no Cl_2) and ALE-regime at different bias set points (RF-power). The results show that a clear EPC plateau for the ALE regime was observed at biases of 20-40 V, corresponding to a peak IEDF Ar+ ion energy of 50-70 eV. The AFM and high-resolution SEM data demonstrated a decreased surface roughness of etched Si in the plateau region, typically for ALE, indicating low surface damage.

Populärvetenskaplig sammanfattning

Föreställ dig att du försöker skala ett äpple, men i stället för att använda dig utav en kniv för att skala äpplet använder du dig utav ett mer effektivare verktyg, för att undvika att skala bort fruktköttet. För att skala äpplet så tunt som möjligt skulle du behöva ta bort skalet ett litet lager i taget, gärna så tunt som möjlig, så tunt som till fristående atomlager. Detta liknar vad forskare gör med ”Atomic layer etching” inom nanoteknik. ”Atomic layer etching” är en mycket exakt metod för att avlägsna material lager för lager, ner till atomnivån. Det är som att skala ett äpple, men i detta fall består varje lager av atomer. Denna precision är avgörande för att tillverka små enheter som datorkretsar, där varje atom spelar roll när vi kommer ner till nanometerprecision. Men att uppnå denna nivå av precision är inte helt enkelt. Traditionella maskiner tar oftast bort mer material än önskat eftersom systemen som använts inte är gjorda för borttagning av enskilda atomlager och tillför alldeles för mycket energi än vad som behövs och skadar ytan på materialet. Tänk dig att försöka skala ett äpple försiktigt med en motorsåg i stället för en kniv – du kommer förmodligen att ta bort mer än bara skalet, men samtidigt kommer det gå mycket snabbare att ta bort skalet. Det är här ”Quasi-Atomic layer etching” kommer in. Det är en modifierad version av ”Atomic layer etching” som försöker hitta en balans: det är inte perfekt exakt, men mycket bättre än traditionella metoder och orsakar mindre skada.

I detta projekt arbetar vi för att göra ”Atomic layer etching” ännu bättre. Genom att använda klassiska halvledarmaterial som kisel arbetar vi för att ta bort atomlager med minimal skada för att förbättra ytkvaliteten. Kisel är ett nyckelmaterial i elektronik, så att göra dess yta så slät som möjligt är viktigt för att tillverka bättre och snabbare enheter. Efter ”Atomic layer etching” undersökte vi kiselns ytor med avancerade tekniker som atomkraftmikroskop och svepelektronmikroskop Dessa metoder användes för att se och mäta hur släta ytorna var och kontrollera eventuella skador.

Genom att förfina dessa tekniker hoppas vi på att fullända ”Atomic layer etching”, vilket gör det till en mer pålitlig och mindre skadlig metod för tillverkning utav halvledare komponenter. Detta är som att hitta det perfekta sättet att skala det där äpplet med en precisionskniv i stället för en motorsåg, vilket säkerställer en jämn och felfri yta varje gång. I huvudsak banar detta arbete väg för att skapa mindre, effektivare och kraftfullare elektroniska enheter som är nödvändiga i vårt dagliga liv, från smartphones till datorer. Genom att bemästra konsten att ta bort material, atom för atom, skjuter forskare fram gränserna för vad som är möjligt inom teknologin.

Acknowledgement

I want to express my gratitude to AlixLabs for giving me the opportunity to work on an amazing project with them. I am especially thankful to my supervisor, Mohammad Karimi, for taking me in and providing continuous support and valuable input. I would also like to thank all the employees at AlixLabs: Jonas, Dmitry, Yoana, Reza,

Asif, Intu, Fabian, and Sungyang, thank you for your amazing collaboration. Additionally, I am grateful to my supervisor, Ivan Maximov, and co-supervisor, Sabbir Ahmed Khan, for their assistance with the project's theoretical aspects and their feedback on the manuscript and the presentation.

Chapter 1

Introduction

The micro- and nano-electronics industry is highly competitive, constantly driving to reduce critical dimensions. This requires developing damage-free, atomic precision techniques for micro- and nanoelectronics materials. This is essential to ensure the continued advancement in the fabrication of semiconductor technology, according to Moore's law. In recent years, Moore's law has reached its limit because the progress in increasing the number of transistors has slowed down due to the available technologies that could not manufacture transistors in smaller sizes than we have today. Fabrication of transistors at the sub-nanometre or even the atomic scale is necessary for the continuous advancement of transistors as per Moore's law. This involves using precise, controlled, and selective processes to achieve the desired properties of the transistor material when working at the sub-nanometer or atomic scale. When doing this it is vital to ensure the integrity and performance of transistor materials. When transistors are reduced to sub-nanometre or atomic scale sizes, the devices will have a larger surface area compared to bulk materials. Therefore, It is crucial to control manufacturing procedures to prevent the introduction of defects, which can negatively impact the optical and electrical properties of the devices. This becomes more challenging when even a single misplaced atom can significantly impact the material's properties. Therefore, there is a need in semiconductor fabrication to search for new materials or technologies to reach the sub-nanometre or even atomic scale.[1]

Atomic Layer Etching (ALE) is one of the most promising techniques for further reducing transistor sizes in a controlled and selective manner. Due to its layer-by-layer control over the etching rate of the etched materials.[2] The etching process in the ALE regime can be described as a self-limiting mechanism where a layer of reactive gas is adsorbed onto the surface of a semiconductor material and reacts with the substrate atoms to remove them in a controlled manner. This spontaneous chemisorption process removes surface atoms upon external stimulation with sufficient energy. Such external activation, which provides sufficient energy for the chemical reaction, can be a bombardment of the surface with low-energy ions produced by the plasma. Those ALE steps form the etch process cycles, which were repeated to remove the necessary material. Achieving high control of etching in pure ALE involves removing a single monolayer (real ALE) or a thin layer through ALE assisted by high-energy ion bombardment sputtering during the etch step or chemical etching when introducing a chemically active species.[2] Other processes that can contribute to the etching, e.g., high-energy ion bombardment sputtering or reactive ion etching, resulting in a

non-perfect ALE, are known as Quasi-ALE (Q-ALE). A Q-ALE can be characterised by removing more than a single monolayer of material per cycle and does not have self-limiting steps. In most cases, the Q-ALE process is plasma-assisted and impacts the etching process differently from real ALE due to the increased contribution of ion sputtering and spontaneous gas-phase etching.

In response to the demand for the fabrication of advanced semiconductor devices, plasma-assisted Q-ALE has emerged as a promising way of etching, avoiding the surface damage commonly observed in reactive-ion etching (RIE), and at the same time, faster and more effective than the real ALE processes.

The main objective of this project is to evaluate the Q-ALE process and assess the extent and depth of damage caused in Si after a certain number of cycles and different ion energies. This work will compare the results obtained through Q-ALE with the theoretical values obtained from molecular dynamic (MD) simulations.[3][4][5] To do this, we have used an in-situ Retarding Field Energy Analyser (RFEA) to measure the Ar+ ion energy distribution function (IEDF) and the ion flux of our system at different Q-ALE conditions (e.g. RF-power, pressure, etc) to correlate the ion energy with the measured extent of the damage. Measurements of the etched surface by atomic force microscope (AFM) and ellipsometry contribute to a better understanding of surface effects after Q-ALE. For further analysis, SEM and EDS will also be conducted to characterise the visual and elemental composition of the surface. This work is performed in collaboration with AlixLabs AB, Lund, Sweden, and the Danish National Metrological Institute (DFM), Copenhagen, Denmark.

Chapter 2

Theoretical background

The main objective of this section is to explain the processes and theories that will be repeated throughout this project. It will focus on processing techniques for etching semiconductor materials, such as reactive ion etching (RIE), Atomic layer etching (ALE), and plasma-assisted Q-ALE. This section will also explore the possible causes of damage formation by these processing techniques. The main parameters that will be considered and evaluated for the quality of the process are etch rate, etch selectivity, and anisotropy. The etch rate of ALE is crucial to have a well-controlled etching process. It is foremost dependent on the material etched, but also, if using a plasma-based system as RIE, the density of reactive radicals or ions available and the ion energy are as important. It is crucial to have control over the material etched, which is defined as etch selectivity. Etch selectivity can be defined as a ratio between the etch rate of a protective mask and the etch rate of the material (substrate) etched. Etching itself can be isotropic or anisotropic, depending on process parameters. Isotropic etching involves removing material in all directions at an equal rate, creating a rounded profile. Meanwhile, anisotropic etching removes material along a preferential direction (usually vertically), producing sharp corners and edges. Anisotropic etching is preferred for achieving a smooth surface since it results in uniform directional etching.

2.1 Reactive ion etching

The advancements in plasma-based dry etching have resulted in numerous technological breakthroughs and enabled significant process improvements. With the development of plasma etching, sub-micro and nanoscale structures have been realised to reach ultimate dimensions. The most used plasma-based etching technique in nanofabrication today is reactive-ion etching (RIE). RIE is a continuous etching process with a high etch rate. RIE involves both chemical and physical processes. The chemical processes of RIE occur in the gas phase or on the surface, without the involvement of wet chemicals, and take place on the sample surface when the reactive etching.

The physical process involves ionising reactive gas molecules and ion bombardment of the sample surface, both occurring in plasma. Plasma can be loosely defined as partially ionised gases. In a confined space such as a vacuum chamber, the ionised particles collectively create a long-range electrostatic field, which significantly influences the behaviours of these charged particles. The electric field is generated because electrons in the plasma tend to move much faster than ions because of their low mass. The fast-moving electrons impact the chamber wall before ions do, causing the wall to become charged negatively. The negatively charged wall surface pushes other electrons away from the wall, creating a layer of positively charged region where an electrical field is created to accelerate the ions toward the sample substrate. This potential difference between the chamber walls or the substrate and the bulk plasma is called “self-bias”. Self-bias is commonly used to control the energy of the impinging ions (usually measured

as a bias on the substrate holder). The ion bombardment process involves creating ions through gas-phase ionisation and accelerating these ionised ions towards the sample surface, leading to the etching of the surface's outermost atoms by impinging ions.[6]

The imping ions will obtain a certain energy depending on many factors, such as the choice of reactive etching gas, system configuration, applied power, and pressure. Depending on if the process is more physical or chemically assisted etching, the etching will become more anisotropic, respective isotropic. The RIE process thus provides the benefits of highly anisotropic etching due to the directionality of the ions bombarding the substrate surface vertically as they accelerate toward the negatively biased substrate placed on top of the electrode. The degree of isotropic or anisotropic etching is also affected by the self-bias and the gas pressure in the reaction chamber, as it will affect the movement of the energetic ions.[7][6]

The choice of a particular reactive etching gas for RIE depends on the requirement of the specific application and the etched sample. For example, halogen compounds such as fluorine (F) and chlorine (Cl) compounds are the most common reactive gases for etching silicon (Si), which is the substrate element in this thesis. Those compounds dissociate and ionise in plasma to produce highly reactive radicals and ions that can interact with the surface Si atoms to form volatile products, like SiClx of SiFx. In a typical RIE process, an inert gas, such as Argon (Ar), is introduced to the plasma to produce Ar+ ions. These ions are then accelerated by the potential difference and directed to the etched surface, where they enhance the chemical reaction by supplying kinetic energy to break the bonds of the outermost atoms. As an additional benefit, the ions of inert gases also stabilise the plasma discharge and make the etching process more reproducible. Unfortunately, the ion bombardment of the surface by ions often results in radiation damage due to high ion energy, so the control of the ion energy is critical.

The rate at which a material can be etched in RIE is controlled primarily by the density of reactive radicals or ions available and the ion energy. The ion current density or ion flux depends on the charge state of the ions within the plasma, the ion density, and the ion velocity that depends on the bias applied within the RIE system, which are all related to the ion characteristics within the plasma. This, in turn, leads to a higher ion bombardment energy, which negatively impacts the etch selectivity. This becomes a problem when working with sub-nanometre RIE features in nanofabrication, where high selectivity etching is crucial.[6][8]

In summary, the RIE is an etching process that is based on the following principles: (a) chemical reaction of the reactive species generated in plasma (radicals and ions) with the etched material, (b) ion bombardment by the inert gas ions provide directionality and enhance the chemical reactions of etching. Those two processes work together; for example, the rate of surface chemical reactions, which determines the etch rate, is accelerated by the ions, and the presence of the reactive species improves the ion sputtering. A pure chemical reaction will typically lead to a slow, isotropic etching, while the ion sputtering will yield poor selectivity and re-deposition of the material elsewhere. RIE is a combination of these three factors, and all of them are interdependent.[7]

In the case of RIE etching Si by Ar+ ions that will be used in this project, calculations by automatic simulation models show that the value of the Si-Si binding energy is estimated to be 3.4-6 eV.[9][10][11] Articles have shown how silicon reacts when hit by ions at different energy levels. The threshold for when sputtering significantly starts happening is

at about 20 eV according to molecular dynamic simulation models and closer to 40 or 50 eV for real experiments.[12][4][13][14]

2.2 Atomic layer etching

Atomic layer etching (ALE) is a process that removes materials layer by layer. ALE removes one atomic layer at a time in a cyclic manner, making it a non-continuous process divided into cycles. To etch a material, it must be exposed to a suitable process gas that decreases the binding energy of the outermost surface atoms. After exposure, any excess gas that has not reacted with the surface must be removed. This ensures that the process gas only affects the surface atoms and not the bulk material. Once the process gas is no longer present on the surface, the etching process will stop on its own. This self-limiting process allows for repeated etching steps without interference from previous ones, relying foremost on the supplied process gas to lower the binding energy for etching. The self-limiting behaviour of ALE makes it a highly controlled process that can be plasma-, thermal-, photon-enhanced, etc. The difference is how the energy to desorb the outermost surface is supplied.

Except for exceptional control, ALE is also known to smoothen the surface of the etched material after processing, providing uniform and conformal processing if used correctly.[15][2] This means that if a sample with a rough surface is etched using ALE, the surface roughness will gradually decrease during the ALE processing. ALE achieves this by removing individual layers of surface atoms one by one, resulting in a gradually smoothened surface. This can be done after or during the etching process of ALE. To ensure the effectiveness of ALE, it's important to avoid anything that may interfere with the etching process, as this could lead to uneven etching and increased surface roughness.

ALE with poor self-limitation can be defined as Q-self-limited and Q-ALE and will have more contribution of RIE sputtering. Controlling the process layer-by-layer may be less effective than in real ALE processes. This is commonly observed when ALE uses high energy to overcome the desorption energy of the activated surface atoms. In such scenarios, excess energy is provided, which can cause the ALE process to lose its self-limiting behaviour, making it Q-ALE. The excess energy will have higher energy than needed in the process and etch the surface even if it is not activated. ALE is a technique used for etching with exceptional depth control, achieved through a self-limiting layer-by-layer mechanism that separates activation and etching steps. However, it is essential to note that ALE is extremely sensitive to various parameters, including the type and quantity of process gas used and the energy applied during the process.

Each cycle of ALE can be characterised based on four steps: activation, first purging, etching, and second purging (see Figure 2.1). These ALE steps form the etch process cycles, which are repeated to remove the necessary material. For the most efficient ALE, etching must occur only when all individual steps work together rather than individually. In the following section, each step of the ALE process will be explained in more detail to provide a better understanding of the purpose of each individual step. This project will focus on using silicon (Si) as a material and chlorine gas (Cl_2) as an active species; ALE of Si with Cl_2 is only one example of the etching process. Other materials and active species can also be used.

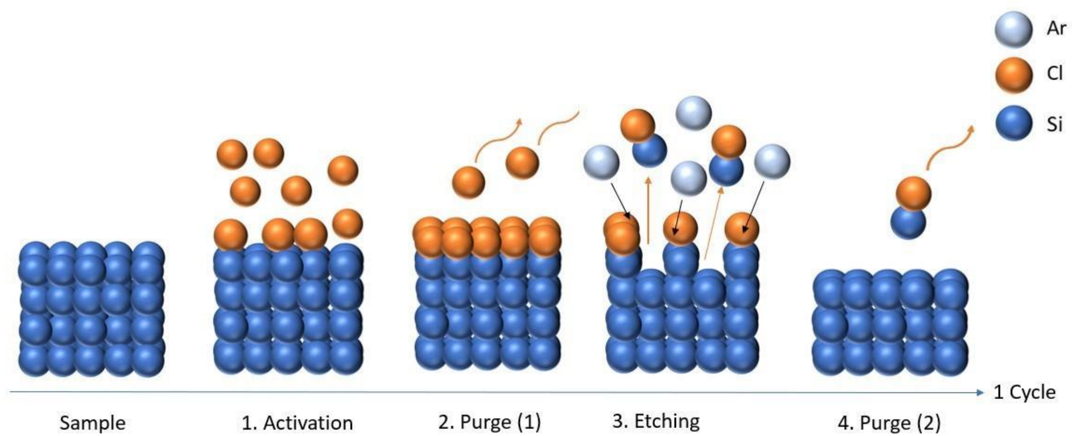

Figure 2.1: A schematic of the atomic layer etching process including activation, purge (1), etching step, purge (2).[11]

2.2.1 Activation (step 1)

The first step in ALE is activation. The purpose of activation is to introduce a chemically active species through an inlet gas to react with the surfaces of the material. With the correct choice of substrate together with dosing gas, ALE can be self-limiting if the chemical dose stops after adsorbing to one monolayer.[16] In the activation step, the gas molecules of Cl_2 are adsorbed onto the sample's surface, forming $SiCl_x$ bonding with the surface atoms. The adsorbed Cl weakens the bonds between surface atoms and the bulk material due to the redistribution of electronegative charge towards Cl, which is more electronegative than Si. The active species must have strong electronegativity for this process to work, creating a polar covalent bond with a partial charge on the electronegative atom. Chlorine is a strongly electronegative due to its seven valence electrons in the outer shell and its tendency to attract electrons to achieve an octet. The strong polar covalent bond of Si-Cl makes it much stronger than the Si-Si bond, making desorption of $SiCl_x$ possible. Desorption occurs when $SiCl_x$ has sufficient energy to desorb on its own or when $SiCl_x$ shifts to its neighbouring SiCl unit and is desorb as $SiCl_2$, as

in $2SiCl(s)=Si(s)+SiCl_2(g)$.[11] Calculations show that Cl_2 gas during the activation of targeted Si atomic layers can effectively reduce the energy barrier of the surface atoms. However, different calculations and models yield varying estimated binding energy values and corresponding desorption energy for Si, $SiCl$, and $SiCl_2$ t. Still, the value of the desorption energy of a silicon atom can be reduced from 7.40-8.46 eV to 1.40–3.20 eV if $SiCl_2$ is formed, and 4.52–5.74 eV if $SiCl$ is formed, the product of the silicon chloride.[9][10][11][7]

2.2.2 Purging step (step 2)

After the activation step, the excess chlorine that has not reacted with the substrate surface is purged from the reaction chamber to prevent any modification to the etched surface during a longer activation period. Suppose the substrate surface is exposed to Cl_2 for a longer period of time, and not all of the Cl_2 has been purged out of the reaction chamber. In that case, this leads to surface contamination due to the contribution of reactive ions during etching, where both the activation and etching processes occur simultaneously. Ideally, the purging time should be as short as possible to reduce the cycle time and chlorine gas waste but sufficient to remove all excess Cl_2.[2]

2.2.3 Etching step (step 3)

The etching step comes after the activation and the first purging step. In the etching step, Si is etched by removing the $SiCl_x$ layers on the outermost surface. Ideally, this means that the surface will need to be activated before it can be etched. Due to its nature, real or pure ALE is a self-limiting process because it can ideally only etch the $SiCl_x$ active surface. This enables ALE to offer exceptional control of the etching rate. In the ideal case, the amount of etched material should be one monolayer per cycle, i.e., one single layer of $SiCl_x$. By removing one monolayer of Si atoms per cycle, the process will maintain the integrity of the material after removing the $SiCl_x$, and the process will be able to be repeated as it was before evenly. The theoretical thickness of a monolayer of Si (100) is 1.36 Å.[17][18]

By breaking the $SiCl_x$ bonds to the surface and removing the reaction product with sufficient energy, the underlying layers maintain the material's integrity. To remove the reaction product, sufficient energy is needed to overcome the binding energy between the SiClx and the bulk. Breaking these bonds can be accomplished using thermal energy, kinetic energy of ions and atoms, or other energy sources such as photons. However, to ensure the optimal efficiency of this process, the energy of surface atoms bonding to the gas must be lower than that of bonding atoms found in bulk.[19] This theory oversimplifies the surface structure and reaction kinetics. It ignores factors such as amorphous or damaged surfaces and chemically active species, which complicate this ALE process of removing single atomic layers. However, it is a good enough approximation for this project

description.[19] It is important that the underlying layers of Si are not affected by the process so that they can repeat themselves in the same way as before when the surface layer is removed. In this case, the total etch depth will be proportional to the number of cycles and etch per cycle (EPC). The EPC is one of the basic characteristics of an ALE process, usually measured in Ångström (Å), or nanometre (nm). When the etching step achieves this sort of etching, it is known to be conducted within the so-called "ALE window," which means providing enough energy to overcome the desorption energy but not so much so that the bulk atoms get affected. Thus, the integrity of the unmodified Si after removing the SiClx surface layer is maintained. The ALE window is typically plotted as EPC versus the ion energy, or if the ion energy is unknown, versus RF-bias power or bias.

The ALE etching step can be divided into three different regimes. The first regime is characterised by incompletely removing the activated surface material at low energy below the irradiation energy threshold for desorption. Active species cannot completely remove the modified top monolayer in this regime.[20] The second regime is the earlier mentioned ALE window, where the etch per cycle is independent of ion energy. This is because the energy provided is only sufficient to remove activated surface atoms, which is a self-limiting process, while a non-selective sputtering is absent or negligibly small. The third and final regime occurs in a high-energy region where the irradiation energy of ions is greater than the desired and can contribute to RIE sputtering. In this region, the process does not exhibit self-limiting behaviour. This is due to the loss of selectivity to the material caused by the irradiation energy, leading to sputtering being the dominant etching process. The selectivity here means the selective removal of a modified top layer with respect to the bulk atoms. At high energy, there be enough chemical and physical species with sufficient energy to impact the substrate material to a greater depth and remove multiple monolayers of material within any given cycle, and the process will lose its selectivity.[20]

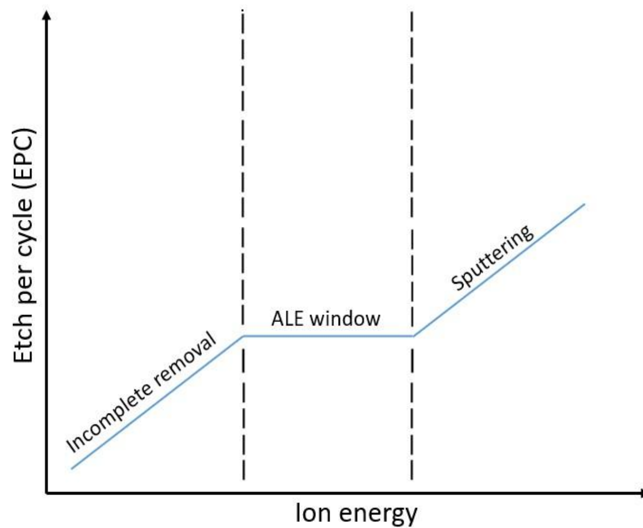

Figure 2.2: Etch per cycle vs. ion energy represents the expected dependence in cyclic etching processes. The three parts represent the incomplete etching of the activated surface material, the complete etching of the ALE window where the etch per cycle is independent of ion energy, and the sputtering regime.[21]

At room temperature, the etching step is the most dominant part of the etching process. However, etching also occurs at elevated temperatures during the activation step. Using temperature alone to provide the desorption energy in this step would require many years at room temperature due to insufficient energy to break the outermost bonds of Si. To speed up the chemical reaction rate, we utilise directional and more efficient etching by using an inert gas plasma, like *Ar*, which provides sufficient energy to break the outermost bonds.[2] Plasma-assisted ALE is also known as plasma-assisted Q-ALE or PA-ALE; in this project, we will use the term Q-ALE. In the plasma process, a chemically nonreactive feed gas flows, as Ar, into the RIE discharge reactor, where the discharge electrons dissociate the feed gas and produce reactive species, such as $Ar+$. Q-ALE is a cyclic etching process, like real or pure ALE, but the process is also Quasi-self-limiting. Quasi-self-limiting means that the etch rate is not zero after removing the activated layer, and longer times of the etching step will result in an increase in EPC. In Q-ALE, high-energy ions will always be the impact that will continue the etching process, whether the Si surface consists of modified $SiCl_x$ or not. Unlike in real ALE, where the etching is stopped when the $SiCl_x$ on the surface is completely etched, the Q-ALE process continues via sputtering by ions that will contribute to the overall etching. Therefore, in plasma-assisted Q-ALE, the “ALE window” will never be completely flat but will instead have a slight decrease in inclination during the Q-self-limiting ALE regime, see Figure 2.3. In practice, the impact of sputtering during Q-ALE cannot be avoided, but it can be reduced by lowering the energy of the ions below the sputtering threshold. Q-ALE assisted by Ar+ plasma and surface activation can provide sufficient

energy to overcome the Si-Si binding energy of 2.3-4.0 eV for activation by Cl_2 gas. However, the approximate calculations of the surface binding energy do not accurately determine the sputtering process after Cl_2 gas.

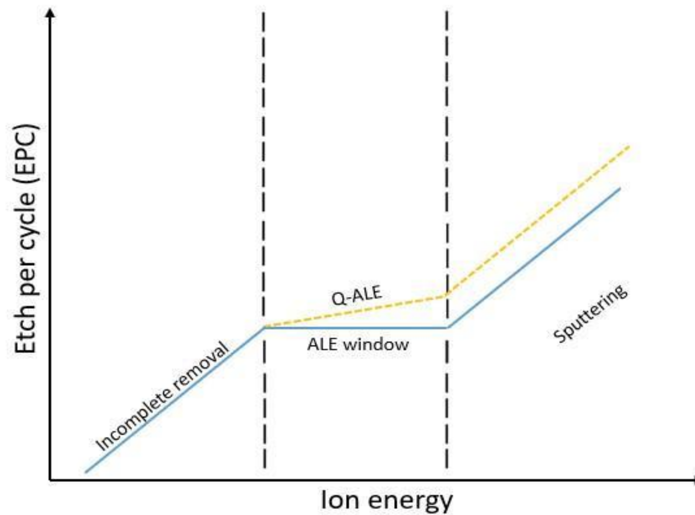

Figure 2.3: Etch per cycle vs. ion energy represents the expected dependence in cyclic etching processes. The three parts represent the incomplete etching of the activated surface material, the complete etching of the ALE window where the etch per cycle is independent of ion energy, and the sputtering regime.[21]

Experimental studies suggest that around 50 eV is typically needed for Si to desorb after Cl_2 gas.[9][10][11] This requirement is about ten times greater than the approximate calculations. This difference can be attributed to the fact that molecular simulations do not account for the fact that the removed atoms must also rebound up and away from the surface. This process requires more energy than what simulations account for, as they only consider the desorption energy and inner collisions of atoms bouncing off each other.[9][10][11]

Limited available studies have been investigating the process of etching silicon under the influence of Ar+ plasma sputtering by Quasi-atomic layer etching at lower energy levels of sub-50 eV. Only a few experimental and molecular simulation models have been published in this area. Most of the published articles are simulation models that go down to low energy ranges of sub-50 eV by using molecular dynamic (MD) simulation or density functional theory (DFT) approaches to investigate sputtering and ALE processes on Si under the influence of Ar+ plasma sputtering with and without Cl_2 gas in the activation step. The results show that by using Cl, the energy threshold for a reaction to occur can be lowered to around 20 eV, according to molecular dynamic simulation models (MD).[12][4][13] However, when looking into articles that compare simulations to experiments, this threshold of 20 eV has yet to be achieved; the lowest value that was found for the ion sputtering threshold by experiment measurements for Si by Ar+ is about 45-50 eV.[12][4][13]

2.2.4 Purging step (step 4)

After completing the etching process, the next step is the etching purge. During this final stage of the ALE cycle, the by-products formed after removing the modified layer are purged to clean the chamber. The purging time should be long enough to be able to purge out desorption products such as $SiCl$ and $SiCl_3$; otherwise, if the time purging is not long enough, some of the by-products will remain inside the chamber and negatively impact the sequential cycle and can lead to additional etching that can alter the etching resolution of the whole process.[5]

2.3 Damage formation

In the previous section, the concept of the ALE window was mentioned, describing the ALE process as being within the ion energy region at which the etch per cycle is independent of ion energy. Outside the ALE window, there is a higher risk that the sample will experience surface deformation or damage. However, the ALE window region is very narrow, making it hard to avoid activation. When a highly reactive ion plasma is added to the process, the process becomes Q-ALE; activation and damage are almost impossible to avoid. Since ALE is both a chemical and physical etching process, both physical and chemical etching can cause activation or damage. High-energy ion bombardment can change the material's crystalline structure, creating defects and interstitial vacancies in the crystalline lattice and changing the chemical composition of the material due to ion implantation or resulting in surface roughness. Damage formation during ALE depends on ion energy and process conditions such as pressure, gas flow, and temperature, which will affect the plasma formation, ion flux, etc. In this section, we will go through possible sources for damage formation of the sample during processing. As we use Si etched by a combination of Cl gas and Ar+ ion bombardment in this project, it will be the only element considered in this section.

2.3.1 Incomplete etching

For low ion energy below the sputtering threshold for the active surface, incomplete etching of the activated surface material is present. This is because the ion energy is not high enough to break the bonds between the activated surface material and completely remove the material from the surface. Incomplete etching after activation can also occur when the energy is sufficient to break the bond between the bulk and the activated surface atoms but not sufficient to remove it far away from the surface for the purge step to remove the volatile products. Instead, the volatile products are redeposited on top of the surface and form new structures on top of the surface during etching. It is also possible that reaction products escaping from the surface can collide with another surface or chamber byproducts, where they can stick or be directed back to the sample surface. Here, the chamber pressure is an important factor; the pressure will determine the particles' mean free path (λ), e.g., how long the particle can travel without colliding with other particles. If λ is long, the particle can travel far enough to be purged out of the system, but if the λ is short, the particles are more prone to interfere with other particles in the chamber and be returned to the sample surface. This means that the molecules or fragments that leave the surface can undergo the reverse process and redeposit onto a surface in the line of sight. To address the redeposited material, the composition of the impacted surface is altered by adding atoms, thereby changing the surface stoichiometry.

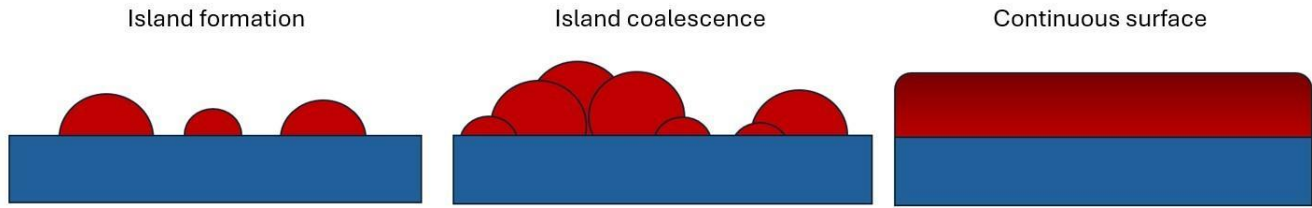

Figure 2.4: Island-layer-island growth. The schematic diagram showing the island-layer-island growth.

After several cycles, the material that has been re-deposited will gradually form into dispersed nanoparticles, which will group through a layer-by-layer competing growth mechanism such as island growth. Over time, these islands will coalesce to form continuous films.[22] Whether the deposited material is single crystalline, polycrystalline, or amorphous depends on the experimental conditions and the substrate. The deposition temperature and the impinging rate of growth species are the most important factors. For low-temperature ALE, redeposited particles do not have enough energy to move and will stay where they were first deposited, forming an amorphous film over time. For the redeposited material to form crystalline or polycrystalline films, the temperature needs to be higher than what is commonly used for ALE, making it more common for redeposited material to form amorphous films. Figure 2.4 shows the schematic representation of island formation forming a continuous surface of redeposited material. It is also worth mentioning that the ion energy in an RIE system is distributed over a wide range of energies, meaning that even if the ion energy supplied is high, some ions will always have lower ion energy that will not be as effective as higher energy ions during etching, more about this when going through ion energy distribution function curves in retarding field energy analyser measurements.

2.3.2 Dangling bonds

Another factor that will enhance the probability of incomplete etching during ALE is the surface itself. Si has a diamond cubic crystal structure. The Si atom has four valence electrons and requires four bonds to saturate the valence shell fully. Each Si atom establishes bonds to its four neighbouring atoms in the crystalline structure, leaving no unsaturated bonds. At the surface of the Si crystal, the periodicity of the crystal is broken, and the surface atoms will not have enough atoms to bond to. The Si atoms will instead rearrange themselves to diminish the number of unsatisfied bonds. The etching of crystal periodicity creates a vacancy that acts as a trap, also called dangling bonds. These traps are formed from unsaturated bonds that cannot be diminished by rearrangement of the neighbouring atoms, leaving free electrons from neighbouring atoms, see Figure 2.5.[23]

After oxidation, most of these vacancy traps are saturated with oxygen atoms, but for a process like ALE, where a new surface is forming for every cycle, and no oxygen is present, dangling bonds make the Si surface highly reactive to active species within the ALE process. This will affect the etching of ALE since active species and etch products will be strongly attracted to these dangling bonds. For a higher number of cycles, this can hinder the continued etching; if

active species are not purged out or rest products within the system are bonding to dangling bonds that will not be affected by the activation etching procedure of ALE, this will form defects on the surface of the Si surface. In Figure 2.5, one can see a schematic of the possible outcomes of free unpaired electrons on the outermost
surface.

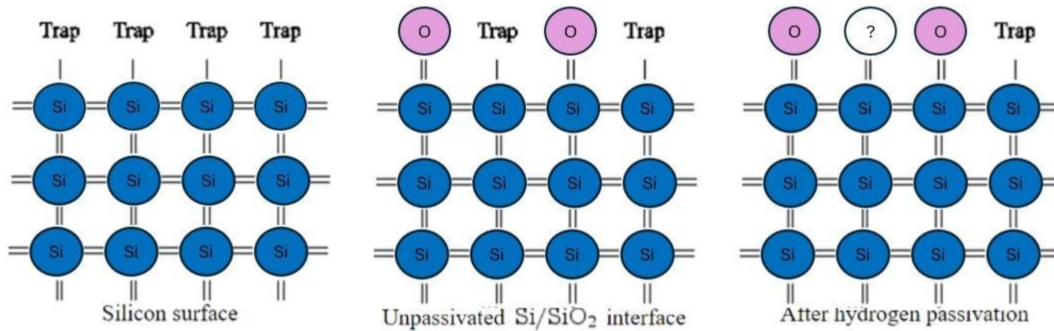

Figure 2.5: (a) At the silicon surface, silicon atoms are missing, and unpaired valence electrons exist, forming electrically active interface traps. (b) After oxidation, most interface states are saturated with oxygen bonds. (c) If the volatile product is not completely removed after etching, it will be attracted to form bonds with the dangling bond surface [23]

2.3.3 Sputtering

For RIE, sputtering by ions will always be present, and for higher energies, it will significantly contribute to the etching process. The sputtering occurs when the irradiation energy exceeds the desired energy levels for ALE, causing the ALE process to lose its self-limiting behaviour and selectivity, see Figure 2.6. Figure 2.6 shows etch per cycle/etch depth versus plasma etch time for a self-limiting process, a Q-self-limiting process, and a continuous process of RIE sputtering. Sputtering during RIE can damage the substrate when the energy of the ions during processing reaches 50-500 eV; at this energy level, the ions will most likely only penetrate a few nanometres. However, damage can be introduced deep into the structure, up to 100 nm, due to the effect of ion channelling caused by the favourable orientation of a crystalline structure. This occurs when the ions intersect with an aligned crystalline structure so that its single layers do not hinder the movement of the ions. These aligned structures create pathways within the material that allow for uninterrupted movement of the ions without any opposing forces. It is generally believed that due to uninterrupted pathways, damage is introduced into the crystalline structure by traps, vacancies, and interstitial atoms.

Reducing the ion energy is the most effective way of reducing the damage. Low ion energy will reduce the RIE sputtering directionality, making it harder for the ions to travel between crystalline structure channels. However, the damage thickness from the surface down to the bulk is consistent with the Ar+ ions penetration depth. Even in the case of ALE, the lower ion energy is required to minimise the ion-induced damage. Experiments show that ion penetration-induced damage can be controlled below 50 eV.[24] If the supplied RF is decreased in the RIE system, the

ion mobility and concentration at the etched surface also decrease. To reduce surface damage, inductively coupled plasma (ICP) can also be used within the RIE system (ICP-RIE).

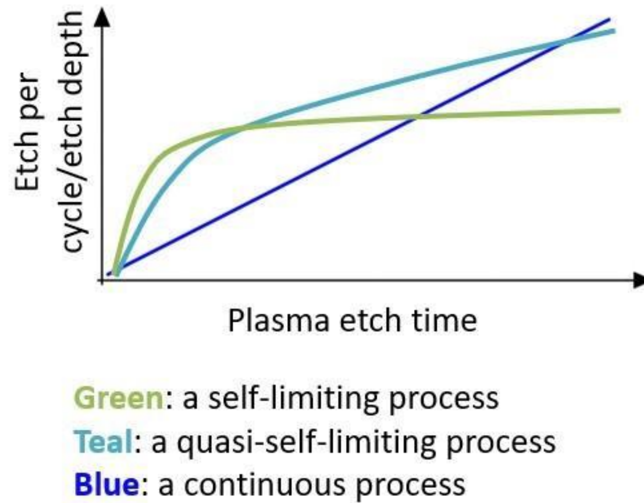

Figure 2.6: Etch per cycle/etch depth versus plasma etch time for a self-limiting process (green), a Quasi-self-limiting process (turquoise), and a continuous process (blue).[21]

The use of ICP can help control the ion bombardment energy by adjusting the substrate stage bias voltage. However, reducing the RF power also changes other conditions to maintain the necessary etch rate, selectivity, and anisotropy.[25]

Sputtering-induced ion damage can also present in the lower energy range of less than 50 eV but to a much lesser degree. For an ICP-RIE system, the ion energy is distributed over a wide range of different energies, meaning that even if the ion energy supplied is low, some ions will always have a higher ion energy that will contribute to sputtering. When higher energy ions are present, the high-energy ions penetrate deeper into the sample, increasing the damaged layer thickness from the surface to the bulk. The degree of damage will also depend on factors such as chamber conditions, exposure time, etc. and most importantly, ion energy. The near-surface crystal structure will inevitably be disturbed by ion bombardment when exposed to energetic ions with energies above about 10 eV.[4] The damage thickness is consistent with the ion penetration depth for low-energy ions. When considering ALE molecular dynamics (MD) simulations, it shows that the chemical modification species can be mixed into the amorphous damaged layer of Si during ion bombardment. This is causing additional complexities in the ALE process because it causes changes in the chemical structure in the near-surface region that will vary with both time and depth. MD simulations have revealed that in a Si atomic layer etching process utilising Cl_2 gas and Ar+ ion bombardment by plasma-assisted ALE, the Si etch rate decreases as the Ar ion flux (mA/cm^2) increases. This decrease in yield is due to the Cl_2 gas and other active species; content in the near-surface region also decreases as a function of the Ar ion flux. The MD simulations

show that the Cl atoms are present in the amorphous damaged Si layer in interstitial sites throughout the damaged Si layer. Additionally, there is a significant change in etch product yield during the ion bombardment step. At the beginning of the step, the Cl and $SiCl_x$ species dominate product distribution. However, the yield of these products quickly decreases with increasing Ar ion flux, while the atomic Si yield remains constant throughout the cycle due to physical sputtering. To minimise physical sputtering and ion-induced damage, you must have control of not just the energy of the Ar ion but also the ion flux of the Ar ions.[4]

Plasma-based Ar sputtering has also been found to increase the formation of native oxide during processing due to the contribution of SiO_2. This oxide has been shown to decrease the etching rate of Si, forming a coalescence layer on top of the etched Si that grows with plasma exposure time. In the case of a plasma with an ion energy of a maximum of 15 eV, surface analysis confirmed higher levels of oxidised Si on the surface after Ar+ sputtering. According to studies [26], increasing the energy to 30 eV also seemed to accelerate reoxidation. Since no oxidation is observed without plasma, the energy dependence indicates ions as an important component of plasma that enables oxygen in the chamber to oxidise the Si surface. This ion-enhanced reoxidation of the Si surface can occur even with very low oxygen levels present for this process chamber without environmental exposure that would introduce O_2 and H_2O. Several previous studies suggest an erosion of the quartz coupling window as a source of oxygen for inductively coupled plasma systems.

Chapter 3

Method

3.1 Experimental tools and conditions

3.1.1 Inductively coupled plasma-reactive ion etching

Reactive ion etching (RIE) is a complex process. This section will describe a qualitative and simplistic description of the RIE tool and what is happening inside the plasma etching chamber. The cyclic etching processes were performed in an inductively coupled plasma (ICP) reactive ion etching (ICP-RIE) system Apex SLR from Plasma-Therm LLC (re-branded ICP-RIE Takachi *(TM)*).[27] For this project, we will rely solely on RIE using the ICP-RIE system. The ICP source relies on plasma formation via an inductive coupling that provides a high-density plasma discharge. However, its detailed description does not apply to this project and will not be discussed further. Instead, we will describe the system using RIE. The RIE Apex SLR from Plasma-Therm LLC comprises two main parts: a plasma process module where the etching takes place and a load lock to transfer samples inside the reaction chamber without breaking the vacuum. Figure 3.1 presents a generic plasma processing system consisting of a load lock, plasma process module chamber, RF power supply, pressure gauge, and vacuum pumps.[28]

The plasma process module and the load lock are pumped down to a high vacuum for processing. They are connected to a nitrogen gas (N_2) source for venting, which means filling the chamber with gas until atmospheric pressure is reached. The plasma process module is connected to the load lock through a door, which transfers materials using a mechanical arm. Inside the chamber, the sample is placed on three rods in the plasma process module and secured with a mechanical clamp when processing. The clamp has an opening defined as the wafer's exposed surface. The sample is provided with helium (He) backside cooling at a constant He flow from an external source during processing. The plasma process module has two gas inlets, one for venting N_2 and one for processing. The gas system allows the use of several process gases. The gas flow is controlled by a mass flow controller (MFC), which can adjust the flow rate of the process gases in each gas line. An outlet connected through a throttle valve to a turbo pump and mechanical pump is on the bottom of the plasma process module. The position of the throttle valve adjusts the operating pressure by changing the pumping speed. It is controlled by a capacitance manometer of a membrane type.[21] Plasma inside of the plasma process module can be generated in a range of pressures in

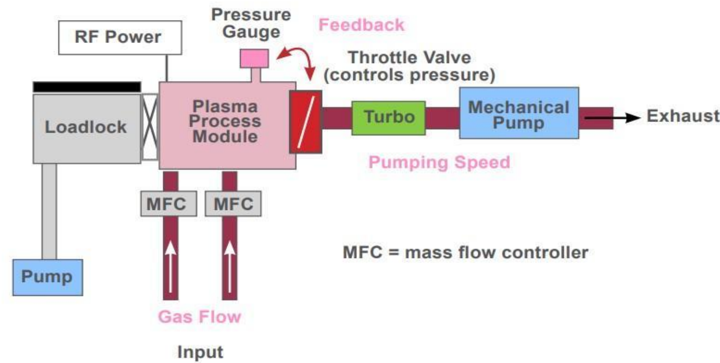

Figure 3.1: Simple schematic of a typical plasma etching system provided by Plasma-herm [28][29]

the RIE system, from atmospheric to vacuum. However, to achieve high-precision etching, such as sub-nanometre etching, it is necessary to maintain a well-controlled plasma environment, which requires a well-controlled vacuum. Therefore, a vacuum pump is incorporated to exhaust the process gases and maintain a stable environment within the plasma process module.[28]

The plasma process module also consists of two electrodes; one electrode is the cathode, which is connected to a radio frequency (RF) power source by capacitance coupling. The second electrode is the grounded anode, including the reaction chamber walls. The RF power source provides a high-frequency electrical field between the anode and the cathode, accelerating the plasma's free electrons. These electrons will acquire kinetic energy in the high-frequency electrical field, and when the electrons have gathered enough kinetic energy, they ionise the gas molecules during collisions. When more free electrons become available, and more gas molecules are ionised, the gas-filled space between the cathode and anode changes from insulators to conduct such electric currents that can flow between the electrodes.[6]

A large part of the region between the electrodes is an equipotential region, also called the glow discharge region. In this region, electrons and ions recombine to form molecules. During this equipotential region, the gas molecules go from an excitation state through recombination to a neutral state, releasing energy as photons. During this recombination, a glowing light is seen in the plasma chamber. The high-frequency electrical field near the cathode and anode is formed because of the fast-moving electrons and charging of the electrode surfaces. The region near the ungrounded cathode establishes a higher potential difference between the substrate and the bulk plasma, also known as self-bias, accelerating the ions toward the cathode. Therefore, a sample placed on the cathode electrode will experience a bombardment of high-energy ions, as shown in Figure 3.2.[6] A matching network is inserted between the RF source and the powered electrode to protect the RIE system from possible damage due to impedance variations. The matching network pairs the RF into the plasma through impedance matching more efficiently.

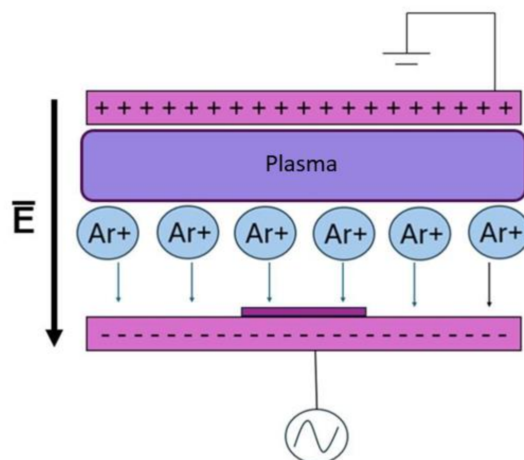

Figure 3.2: A schematic of the reactive ion etching process of the physically accelerating Ar+ ions by the self-bias generated by the radio frequency (RF) power source*. [11]*

The impedance matching protects the source from reflected power back into the source and provides a blocking capacitor. This blocking capacitor and the inequality of electrode areas generate a bias on the powered electrode or cathode. The bias is important, as previously mentioned, to achieve high sub-nanometre control by RIE; a number of parameters can be externally varied to get high precision control, such as gas flow rate, RF power, chamber pressure, substrate temperature, and substrate bias voltage. These measurable parameters are decisive in providing etching quality, such as etching selectivity and anisotropy, etch rate, and etch uniformity. The control of an RIE process is to adjust these parameters experimentally to match them with a desirable outcome from the above indicators. Though theoretically predicting a plasma etching process is difficult, there are some broad guidelines with which a user should be able to anticipate what happens when certain process parameters are changed. The following sections briefly describe these guidelines for optimising the RIE system.[7]

Flow rate of reactive gas

The process of RIE and ALE depends on the gaseous ion reacting with the substrate surface, converting the surface material into volatile product gases. The reaction rate is directly linked to the supply rate of reactive gas. If the flow rate of reactive ion gasses at constant pressure is too fast, the dwelling time of gas molecules in the reaction chamber can be too short, leading to nonuniform etching. If plasma discharge bias is not increased accordingly, the reactive gas ions generated in the reaction chamber will decrease, reducing the etching rate. However, if the gas flow rate is too low, the consumed reactive gases cannot react with the surface sufficiently, which again can lead to a drop in the etching rate.[7]

RF power

Increasing RF power will increase electron energy and ion energy, creating a more energetic plasma. High RF power will also increase the plasma density, i.e., the concentration of electrons and ions, which will result in a higher rate of ion sputtering, reducing etching selectivity. Sputtering is also known to cause damage; the effect of damage due to high-energy sputtering has been discussed in the theoretical background on surface damage. [7]

Chamber pressure

RIE normally takes place under low-pressure conditions. The chamber vacuum usually ranges from 10^{-3} *to* 10^{-1} *Torr*. At low pressure, the density of gas molecules is low in the chamber. This will contribute to the fact that ions within the system have a longer mean free path (λ), meaning they can travel further without colliding with other molecules. This will result in the gas molecules acquiring more accelerating energy and increasing ionisation probability. The lower chamber pressure results in less lateral etching and better anisotropy. It also leads to a higher pumping speed, which helps to remove volatile products quickly. This, in turn, improves the reaction rate and etching rate. At lower chamber pressure, RIE can be dominated by ion sputtering etching due to the low concentration of chemically reactive gaseous molecules and high ion energy. However, if the pressure is too low, the plasma cannot be sustained, and etching will not be achieved. When the chamber pressure is high, the etching process is dominated by chemical reactions. This is because the ion λ is reduced, and the number of chemically active ions increases. Chemical etching typically results in more isotropic etching. With high pressure and small λ, ions in the plasma are expected to collide more frequently. When ions collide, they lose energy. The higher the pressure, the more dominant this energy loss becomes; if the pressure is too high, the energy loss of the ions will cause the etching process to stop completely. An optimum pressure can optimise the etch rate and selectivity.[7]

Substrate temperature

Generally, high temperatures can promote chemical reactions and help remove reacted products from the substrate surface. The ion bombardment of the substrate will naturally cause a rise in substrate temperature. The substrate surface temperature can reach $100\ C^{\circ}$–$200\ C^{\circ}$, depending on the etching duration. When the substrate temperature is high, there is an increase in lateral etching because the mobility of radicals is enhanced at high surface temperatures. This leads to chemical etching, which is inherently isotropic. To prevent this, the sample holder must be cooled down for longer etching times to reduce the substrate temperature.

Reactive gas

Although the self-bias accelerates ions, causing physical sputtering of the sample, ALE's most dominant etching process is caused by a chemical reaction. Most RIE processes use halogen-containing gasses such as fluorine (F), chlorine (Cl), bromine (Br), and iodine (I) to generate the plasma because they are the most chemically reactive and erosive gases when it comes to inorganic materials. The choice of etching gas depends on the requirements of a specific application. Halogen gases such as F_2, Cl_2, Br_2, and I_2 are commonly used because they are highly reactive when

dissociated. In plasma, these gases dissociate and create a large concentration of the element in an excited state. This excited state reacts with the material on the sample surface. However, if the gases are not dissociated by the plasma, they will not react with the material. When selecting a reactive gas, it is important to choose one that can create volatile products that can transfer from the sample surface and not interfere during continued etching.[6]

Gas additives

Although halogen compounds are the main gases for etching inorganic and metallic materials, additive gasses are often used to enhance some aspects of the etch chemistry. For example, adding 10% O_2 to CF_4 increases the etch rate by 10 times. In the plasma, CF_4 is broken down into radicals CF_3 and CF_2. Without oxygen, these radicals can recombine into stable molecules, such as CF_4. With oxygen present, it can react with the radicals to form CO, CO_2, and COF, thus releasing fluorine radicals that will increase the etch rate. However, selectivity can be substantially reduced because oxygen is an effective etching gas for polymers. Ar^+ can also participate in physical sputter etching to help stabilise the plasma. For example, SF_6 is an electronegative gas. It absorbs electrons upon ionisation, which reduces the total number of electrons in the plasma. The addition of Ar can add electrons to the plasma when they are ionised, and so helps to produce a stable plasma. However, adding too much Ar can dilute the concentration of reactive gas and cause excessive physical sputtering, which will reduce both the etch rate and selectivity. [7]

3.1.2 Retarding field energy analyser

Retarding field energy analyser (RFEA) is a multi-grid plasma diagnostic instrument for ion energy and ion flux measurements at grounded, direct current (DC) biased and radiofrequency (RF) biased surfaces in contact with a plasma discharge that is part of a Semion multi-system from Impedance LLC, Ireland. The RFEA measures the ion energy distribution function (IEDF) and ion flux present at the substrate surface in real-time using an imitation substrate with an integrated sensor. The RFEA is a plasma diagnostic tool that can measure high-energy ion bombardment at the substrate surface, which strongly influences the performance of plasma-based processes. Throughout the process, plasma species bombard the substrate surface, including energetic ions that remove or etch layers of material. The ion impact can directly drive the etching or activate the surface for more reactive plasma species for continuous etching, as is the case for ALE. In the semiconductor industry, the ion flux and associated IEDF are crucial parameters that determine the etch rate, selectivity, and anisotropy. Therefore, measuring, understanding, and controlling the ion flux and IEDF is critical to ensure optimal process performance. The Semion RFEA used in this project offers Energy resolution down to 1eV.[30]

The RFEA Semion multi-imitation substrate is installed in the plasma chamber and is connected to the Semion control unit (SCU) data acquisition system through vacuum feedthrough. The sensing elements and imitation substrate are made of aluminium and can have up to 13 sensors integrated, allowing uniformity measurements. The user configures the SCU using the application software to collect and analyse data. The setup of the system is shown in Figure 3.3. The

SCU data acquisition system is a versatile scientific instrument that provides a controlled high-voltage source and high-precision low-current measurement system connected to a computer for data analysis.[31]

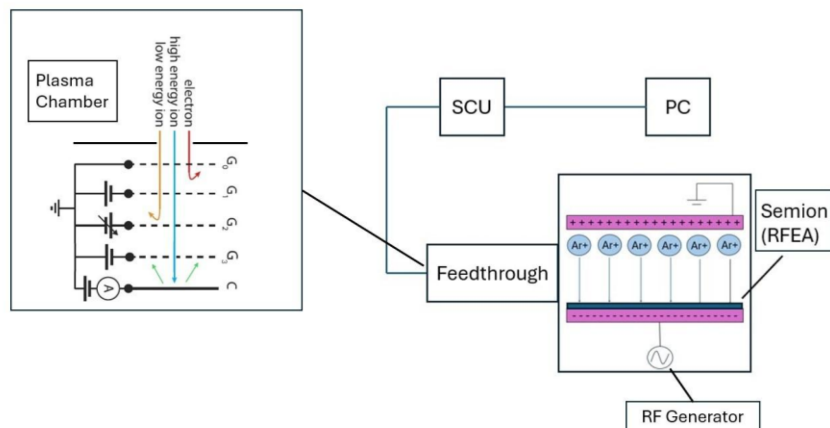

Figure 3.3: Schematic of the RFEA semion working principle from impedance LLC, Ireland. G0 is at wall potential, G1 is biased negatively to repel electrons, the positive bias on G2 can be scanned to select which ions can pass through to the collector C, and G3 have a negative bias repealing secondary electrons (SE) created from the surface to get into the system.

The feedthrough probe sensor is installed inside the vacuum chamber. A multi-core cable assembly passes electrical signals to and from the feedthrough probe sensor. The cable assembly comprises high-temperature wiring protected in a high-temperature sleeve, insulated from the plasma with a flexible ceramic shield. The feedthrough probe makes the interface between the reactor vacuum and the air side. The feedthrough probe enclosure houses the low-pass filter elements inside the system, enabling the sensor to float at the bias potential applied by the tool. The part of the feedthrough probe that interfaces to the plasma chamber has different holes, allowing ions to travel into the feedthrough probe for RFEA measurements. The number and diameter of the holes where the ions can move through are dependent on the sensitivity of the probe. Depending on the probe's sensitivity, different amounts of ions of different energies can be detected. e.g., when using a high-sensitivity probe, all ions will be detected. A low-pass Filter with a high input impedance at the frequencies of interest is placed between a set of insulated grids, a collector, and the RFEA electronics to ensure that the grids and the collector maintain the electrode RF potential. These filters prevent the overloading of the electrode measurement electronics. The feedthrough probe enclosure incorporates the terminals for connecting the RFEA sensor to the SCU data acquisition unit.[31]

The RFEA consists of four grids and a collector electrode to which a negative bias is applied to attract ions for detection to record ion current. The grids are used to filter what ion energies to use. Figure 3.3 shows a schematic of a four-gridded RFEA system consisting of a stack of electrically insulated grids, G0 through G3, and an ion-collecting electrode C. The corresponding potential distribution of the different grids inside the device is also shown in the Figure. The first grid, G0, faces the plasma and has the same electric potential as the surface on which the RFEA is mounted. G1 has a negative potential compared to G0 in repealing plasma electrons. For the G2 gird, an ion retarding potential (V_R) is applied that allows only those ions that have an initial kinetic energy than qV_R to pass at the entrance and reach the

collector of the RFEA, with q being the ion charge. It, therefore, acts as a high pass filter for the ion energy. The G3 grid has a bias of 10 V, which is more negative than the Collector. This grid creates a retarding potential for secondary electrons (SE) that can be emitted from the surface of the collector due to high energetic ion impact.[30]

For the RFEA to measure the IEDF, V_R is swept over a number of energies while measuring the collector current. The IEDF is calculated by taking the derivative of the collector with respect to the retarding potential, where the first derivative in the series is calculated numerically. The ion flux (A/m^2) is calculated by dividing the measured ion current by the effective sample area and the ion charge (we assume only singly charged ions). The effective sampling area is determined by the probe area and the effective transmission of the grid stack, of which the latter is defined as the ion flux density at the collector relative to the flux incident on G0. The ion flux is a good and reliable parameter for comparing different plasma-based systems and molecular simulations since the ion flux is determined by the flux of ions hitting the material's surface. The Semion RFEA system has an ion energy range of 0 to 800 eV, ion flux 0.1 - 2 A/m^2, and IEDF resolution +/− 1 eV nominal.[30][31]

3.1.3 Ellipsometry

Ellipsometry is an optical technique for measuring thin films' thickness and dielectric properties. It has the resolution to measure the layer thickness down to approximately 1 Å. It measures changes in polarisation from a light source as linearly polarized light is transmitted or reflected through a material structure [32]; see Figure 3.4.

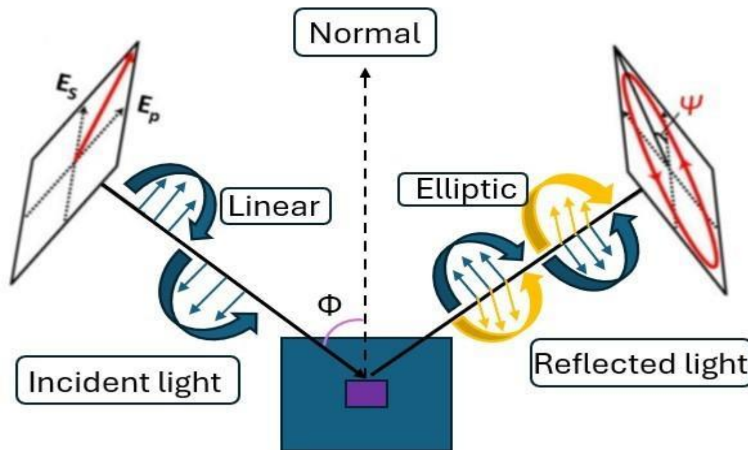

Figure 3.4: Interaction of polarised light with a sample in ellipsometry.

Ellipsometry measures the rotation of the amplitude ratio of elliptically polarised light, denoted by Ψ in the Figure. It also measures the phase difference between E_p- and E_s-polarized light waves before and after reflection, denoted as Δ when they are reflected. Ellipsometry does not measure thickness directly but instead uses an indirect characterisation technique that requires an optical model with fit parameters to compare the reflected polarised light of the measured sample to extract the refractive index and the thickness of the sample.

The optical model is generated according to the prediction of the sample properties based on the optical constant and layer thickness.[32] The deviation from the optical model to the real sample is defined as the mean square error (MSE). The MSE measures how well the model agrees with the measured data. A perfect model fit to the real sample will have MSE = 1. It is important to have an optical model with fit parameters to get reliable data from ellipsometry measurements. The optical properties of a material will vary for different wavelengths and must be described at all wavelengths measured with the ellipsometer. The information from the optical model is then compared to the measurements of ψ and Δ the reflected polarised light from the sample to obtain the reflective index of the material. The typical probe spot size for the collimated beam of the ellipsometer is between 2 and 5 mm in diameter, and the ellipsometry estimates an average over this area for measurements of ψ and Δ.

Once the reflective index is known, the thickness of the material can be determined. In spectroscopic ellipsometry, Ψ and Δ values are acquired as a function of wavelength at different incident angles to maximise the sensitivity of the measurements. Different incident angles where Ψ and Δ exhibit large variation give more reliable model fitting results. The ellipsometry angles become impossible at a normal incidence angle since p- and s-polarization cannot be distinguished.[32] Measuring at three different angles (5 or 10 degrees apart) is recommended. This is important if the sample model has many layers and fit parameters to be measured. Material with a higher refractive index should be measured at higher angles [33].

Ellipsometry is very sensitive to film thickness and uniformity and can be used to investigate almost any transparent thin film or etched surface in the case of ALE. It can be used to measure thin layers or etched surfaces thinner than the wavelength of the probing light itself down to less than a single atomic layer.[34] Ellipsometry can be used to analyse specific sample characteristics, including film thickness, surface roughness, and thickness consistency. A high-quality ellipsometry measurement should show a gradual decrease in the periodicity of model oscillations as the wavelength decreases. If the measurements are noisy and random, the light is likely hitting a film defect or contamination on the sample surface. To get more reliable measurements, it is good to always do measurements at two or more different locations or more on the sample.[33]

The purpose of using ellipsometry for this project has been to characterise the thickness of different layers of the silicon on insulator (SOI) samples used during the project and compare the thicknesses before and after etching. The optical model for ellipsometry has been defined using a trial-and-error approach by fitting the sample's optical constants and layer thickness with ellipsometry software.[32] The optical model has been optimised to fit the manufacturer's description of the substrate and its corresponding MSE from the ellipsometry software. For this project, we have used an ellipsometry optical model consisting of 4 layers consisting of a Si substrate, a SiO_2 layer ($SIO2_JAW2$), a crystalline Si layer (SI_JAW), an amorphous Si layer ($a{-}Si_Aspnes_cl$), and a native oxide layer on the top ($NTVE_JAW2$). The SOI samples used for this project have a 60 nm Si thickness on top of the SiO_2. The ellipsometry optical model of Si comprises an amorphous and crystalline Si layer. The amorphous Si layer represents the damaged layer after etching, which will have different optical properties than crystalline Si. The crystalline Si layer represents

the undamaged Si layer beneath the damaged amorphous Si layer. This will help create a more accurate fit for the SOI sample after etching it to the ellipsometry optical model. The native oxide layer is the oxide that naturally forms on the Si surface over time when exposed to oxygen. While it's something we want to avoid, we cannot neglect it when the sample is subjected to oxygen.

The ellipsometry software fits the parameters for all single layers except the Si substrate despite sufficient etching power to reach underlying layers. This affects the ellipsometry model and makes small variations of measuring the thickness of each layer but should not affect the total thickness of all layers; we are using the total sum of the thicknesses of all layers throughout this project to make the ellipsometry model more consequent and reliable.

However, the model is not perfect, and surface roughness will reduce the optical density at the interface, and this will affect the fitting of the optical model. Unlike methods such as atomic force microscopy, which can image surface roughness, ellipsometry must conclude the level of roughness based on its effect on measurement parameters averaged over the diameter of the probing beam. This can lead to some problems regarding the ellipsometry measurements of surface roughness. Since roughness layers can be very thin and still affect the ellipsometry data, they can be correlated with other surface layers and interfere with the measurement, which is something one must consider when constructing the optical model.[35]

3.1.4 Scanning electron microscope

Scanning electron microscope (SEM) is an imaging technique based on the interaction of electrons and matter.
SEM can be used for surface imaging and object topologies. The operation of SEM involves a cathode (filament or other type) that produces electrons, which are shaped by an electron optical system. Subsequently, the electrons are accelerated by an accelerating electrode and focused on a small spot. For this process to be possible, the sample and the filament must be within a vacuum chamber condition to avoid collision with surrounding gas molecules. The electrons are guided to the sample by a series of electromagnetic lenses converging the electrons to a high-voltage electron beam. In SEM, there are two types of electromagnetic lenses: the condenser lens, which determines the size of the electron beam, and the objective lens, which focuses the beam onto the sample. The resolution and depth of field of the SEM image are determined by the beam current and the spot size, which is determined by one or more condenser lenses together with the probe-forming objective lens. The lenses are also used to minimise the effect of spherical aberration, chromatics aberration, diffraction, and astigmatism, which have to be corrected by aligning the lenses before imaging.[36]

The interaction depth of electrons and the sample occurs within a few nanometres to several microns of the surface before interaction with the atom in the sample. The extent of the interaction volume will depend on the primary electrons accelerating voltage and the material density. After the electrons have interacted with the sample, various

types of signals carrying helpful information about the sample in the form of electrons and X-rays are generated from the sample, see Figure 3.5. For example, if 10 kV, the electron interaction depth will be 1 µm for Si.

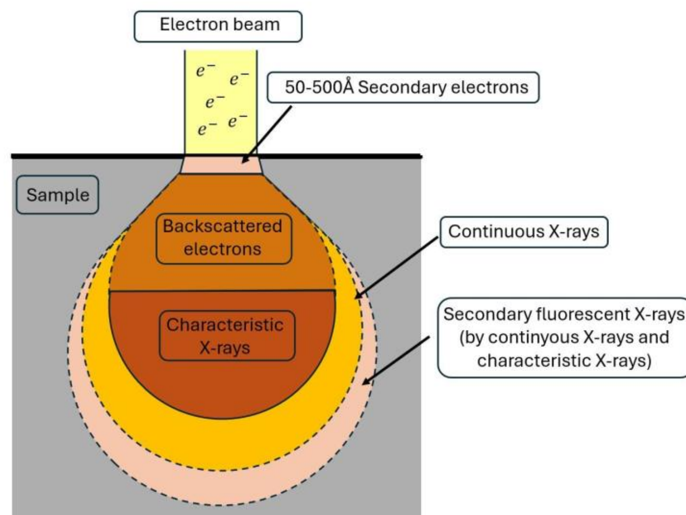

Figure 3.5: Shows the different interaction depths of SE, BSE, Characteristic X-rays, Continuous X-rays and secondary fluorescent X-rays.

In SEM, two types of electrons can be used for imaging: backscattered electrons (BSE) and secondary electrons (SE). BSE is reflected after elastic interactions, i.e., without losing energy between the beam and the sample. BSE has higher energies than 50 eV and comes from deeper regions of the samples. BSE images can provide information on crystallography and topography. SE originates from the surface of the samples and results from the interaction between the electron beam and the sample. SE electrons have lower energy than BSE, typically 50 eV, and provide information on the surface morphology in the 50-500 Å range from underneath the surface. SE is the most common electron used for imaging. Once the electrons escape from the sample surface, they are detected by a photomultiplier detector, creating an image of the intensity of the SE emission from the sample. The photomultiplier detector detects the intensity at each x, y data point during a rastering scan of the electron beam across the surface to create an image.[36]

SEM cannot be used for elemental analysis alone, but it can be used for quantitative elemental analysis when paired with energy dispersive spectroscopy (EDS). EDS is a microanalytic technique used to identify and quantify elements. When working together with SEM, EDS can be used to create elemental maps of the sample. EDS measures the energy and intensity of the X-rays emitted by the sample when it is exposed to the electron beam of SEM. When the high-energy electrons of the electron beam interact with sample atoms, the electrons of the atoms' inner shell will start to get ejected. This leads to the creation of an electron vacancy filled by a higher-energy electron from an outer shell. Excess energy is emitted through X-rays as the outer shell electron moves to a lower energy level. During the process of X-ray emission, unique characteristic X-rays are produced. These X-rays have distinct energies (hv) for each

element, which are determined by the attractive forces between the nucleus atomic weight and respective electron shell, see Figure 3.6. The characteristic X-ray spectrum is extracted by counting all characteristic X-rays emitted from the sample. Each element in the sample gives a different spectrum. The spectrum of the X-ray counts is plotted against X-ray energy and basically consists of different Intensity peaks by EDS. EDS can extract different X-ray energy peaks from each element, depending on which inner shell the electron was ejected from. The energy peaks are indicated by the shell the electron was ejected from (K, L, M, etc.), followed by α or β depending on whether the electron was ejected from the closest or second closest inner shell, respectively. EDS can determine the presence and quantity of different elements in a sample by analysing these characteristic X-ray energy peaks using table values and EDS software. To detect the presence of an element on the sample surface, the accelerating voltage of the interactive electron can have to be adjusted, which will also affect the spectrum of EDS. If the accelerating voltage is low, the EDS spectrum will be more surface sensitive due to the lower interaction depth. However, one should be careful when lowering the interactive electrons energy due to the increasing possibility of mistaken real peaks compared to artefact peaks at lower energies. Peaks detected by EDS software at low energies are subject to occasional mistakes, even on well-separated, high-intensity peaks arising from the surface. These low beam energy microanalysis conditions force the analyst to use low fluorescence yield L-shell and M-shell peaks rather than higher yield K-shell and L-shell peaks typically selected for intermediate and high atomic number elements under conventional high beam energy (above 10 keV) conditions. The EDS used in this project are QUANTAX FlatQUAD from BRUKER and have automated peak identification down to 1 keV. Below this, the EDS software interchange artefact peaks with real characteristic X-rays from outer electron shells.[37][38] [39]

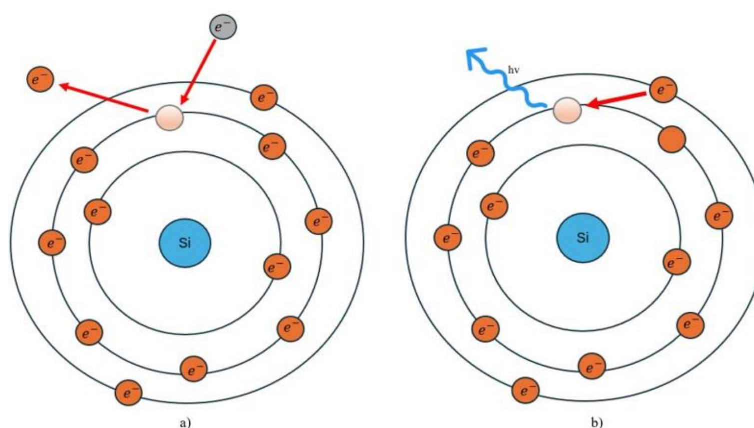

Figure 3.6: The process of creating an electron vacancy by electron bombardment filled by a higher-energy electron from an outer shell.

3.1.5 Atomic force microscope

Atomic force microscope (AFM) is a tool for measuring surface structure with great resolution and accuracy. The AFM scans a cantilever-mounted probe over a sample surface, creating a topographical map of its height. The resolution of

AFM depends on the size of the probe tip radius, which is about 2-5 nm. The principle of AFM is based on measuring forces between the AFM cantilever tip and the sample. Atomic forces cause changes in the cantilever tip, which can be analysed to obtain surface information. The forces between the cantilever tip and sample change as the separation distance changes. As the tip and the sample are gradually brought together, their atoms begin to attract each other weakly. This attraction increases until the atoms are so close together that their outermost electrons begin to repel each other. This electrostatic repulsion progressively weakens the attractive force as the separation decreases. The total force goes through zero and finally becomes repulsive.[40] The separation distance between the cantilever tip and the surface that makes up the perception of measuring the surface topography of AFM is detected by an optical laser. A light beam from the laser diode is deflected off the back of the cantilever onto a position-sensitive photodetector (PSPD). As the cantilever position changes, the position of the laser beam on the detector also changes; see Figure 3.7.

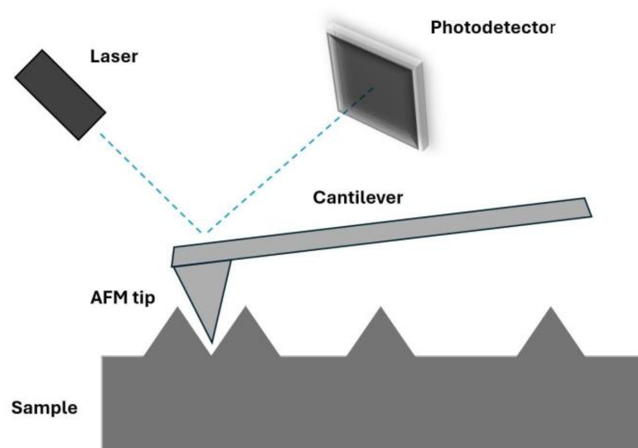

Figure 3.7: Operating the AFM in different force regimes contact, intermittent contact and non-contact mode [40]

AFM has three different force regimes: contact, intermittent contact tapping mode, and non-contact mode. Repulsive and attractive forces and the tip-to-sample separation limit the different force regimes. For contact mode, the tip touches the sample surface, and moving over the surface features causes a deflection in the cantilever. For the intermittent contact mode, the tip briefly touches the surface by an oscillation movement and the lift-off during the continued oscillation. For non-contact, the tip has no contact with the surface but instead oscillates very closely above the surface.[41]

In this project, we are using a Bruker AFM ICON in non-contact tapping mode with the following scan parameters: Scan Size of (10 µm), Aspect Ratio (1), Scan Angle (0 ∘), Scan Rate (1 Hz), Samples to Line ration (512), Lines (512), X (0 µm) and Y Offset (0 µm)

For surface roughness, we are measuring the root mean square average (Rq) of height deviations of the Z-axis taken from the mean image data plane, expressed as the standard deviation of the Z-axis height deviation values of AFM measurement:

$$Rq = \sqrt{\frac{\sum (Z_i)^2}{N}} \tag{3.1}$$

Where Z_i is the current height deviation Z-axis value, and N is the number of points measured during the raster scan of AFM.[40]

3.2 Protocol

3.2.1 RFEA measurements of Ar+ ion energy and flux

This project aims to accomplish plasma-assisted Q-ALE for Si using low-energy ion energies. To achieve this, this project's methodology is based on experimental and theoretical studies that have been proven to determine the ion energy threshold necessary to break the Si-Si surface binding energy. This will allow for the etching of a single atomic Si monolayer from the outermost surface and the successful achievement of ALE. The tool used for this has been an Inductively Coupled Plasma Reactive Ion Etching (ICP-RIE) system from Apex SLR Plasma-Therm LLC (re-branded ICP-RIE Takachi [42]). To obtain accurate measurements, plasma diagnostic characterisation was conducted on the ICP-RIE tool using a Plasma Semion Retarding Field Energy Analyser (RFEA). A high-sensitivity probe sensor was used to measure all ions hitting its surface. The RFEA itself could not be used during the real etching experiments. Hence, the tool was used separately to characterise the plasma discharge and to measure the ion energy distribution depending on the different plasma conditions, such as pressure, RF power, and flow rate, which is the most important condition for our ALE process. The experiment procedure for the Semion RFEA tool was to characterise the plasma under varying pressure and DC bias setpoint, also referred to as bias for simplicity. This allowed us to extract the ion energy distribution curve for different pressures and biases and the corresponding ion flux (A/cm^2) for the given pressure and DC bias conditions. The experiment was conducted at low energy etching region for ALE at increasing biases for 7, 10, 20, 30, 50, 50, 60, 70, 80, and 120 V. RFEA experiments for higher energies were not conducted for higher energy sputtering, for example, that will go up to approximately 300 V bias. This high energy was not taken into consideration during RFEA measurements since it is far above the "ALE window" energy region where ALE is expected. The highest obtained bias used during RFEA measurements was for 120 V with a peak ion energy of 146 eV; therefore, values above 120 V bias will be considered peak ion energy above this value. RFEA experiments were also conducted to increase pressure by 3, 10, 30, and 6 mTorr.

To assure reliable results, RFEA was used for measuring the IEDF with the same parameters but with a 37, 45 min, and overnight break in between and a measurement at the end of all measurements. This is to ensure that the plasma

remains stable and to demonstrate that the data from the Semion RFEA tool remains consistent regardless of when it is used; if not, the IEDF would change depending on when it is used. The results obtained from the RFEA measurements show that the IEDF and ion flux were kept constant for all measurements. This indicates that the RFEA measurements are reliable and can be used independently of the tool condition. The average energy and ion flux standard deviation (stdv) ranges between 0.382 eV and 0.0043 A/m^2, respectively, which is a small error margin that will not affect the reproducibility of the experiments. The RFEA is installed alongside the tool, and various actions, such as leak testing and system pump-down, are taken to ensure that the RFEA is integrated into the tool for reliable in-situ plasma characterisation. When using the RFEA, the RIE is run manually, providing precise control over temperature, chuck, gas, pressure, and RF power. The plasma diagnostic experiments were designed to replicate the ion energy and ion flux parameters used for molecular simulation on ALE for Si, as described in the articles. To ensure that the RFEA measurements are consistent with actual experimental results, we have used the same conditions as for the real experiments with a 2-inch Aluminium (Al) carrier.

3.2.1 Sample preparation and ellipsometry setup

All the samples used for this project are Si on an insulator (SOI) 1x1 cm^2 samples, where the thickness of the top Si layer is approximately 60nm. The samples were diced from a bigger wafer using a Disco Dicer DAD 3320 to achieve the desired size for etching experiments. Experiments were conducted to determine whether cleaning the SOI sample in isopropanol and acetone in the ultra-sonic bath would enhance the cleanliness of the samples after dicing. However, the result showed no significant difference between cleaned and non-cleaned samples after etching, so it was decided that the SOI were used as they were. Before further processing the samples, the SOI thickness is measured by ellipsometry. This is to ensure the thickness of the SOI sample is accurate after dicing. The ellipsometry recipe used for scanning the sample involved taking measurements at five separate locations on the sample. The first measurement location was placed at the centre of the sample, and the other four locations were moved 0.1 cm towards each corner for diversity. The acquisition time for each data point was 2 s. Each location was measured at three different angles: 65°, 75°, and 85°. The wavelengths that we acquired were in the range of 200 to 2500 nm. After scanning the sample surface using ellipsometry, the tool software fitted the data into an optical model.

In this project the ellipsometry optical model consists of four layers on top of the Si substrate, as shown in Figure 3.8. The bottom layer of the optical model is made up of a 150 nm SiO_2 layer (*SIO*2_JA*W*2), a second Si layer (*SI_JAW*), an amorphous Si layer (*a−Si_Aspnes_cl*), and a native oxide layer (*NTVE_JAW*2) on the outermost surface, the total thickness of the *SIJAW*, *a – Si_Aspnescl*, and *NTVE_JAW*2 should be approximately 60 nm. The ellipsometry fits the thickness accordingly to the optical model of all the layers within the optical model except for the Si substrate at the bottom, which has a set thickness since it will not be affected by the etching. The samples were measured by this ellipsometry optical model both before and after processing. To measure the individual single layers and the total etch depth. The etch depth was calculated by subtracting the thickness of the sample before and after etching. This calculation method will be used throughout the project to determine the etch depth and etch per cycle (EPC). Using

the four-layer optical model, we calculated the standard deviation between the five measurement points of each sample. This allowed us to add error bars to the plots made in this project.

After measuring each SOI sample with ellipsometry before etching, they are treated with buffered oxide etchant (BOE), also known as buffered HF. The BOE used for sample preparation comprises a 10:1 volume ratio of NH_4 in water and hydrofluoric acid (HF) in water. This step removes were used to remove any native oxide from the sample before etching, which can interfere with the etching of Si. This is important because Si is the material we study in this project, not the native oxide that forms on top of the Si surface. Before etching, the sample is treated with 30 s of BOE, 30 s of DI water cleansing, and 15 s of drying by nitrogen gun. During the BOE and DI water cleansing treatment, the sample is continuously stirred to ensure even flow over the entire sample surface for uniform etching of native oxide and contamination.

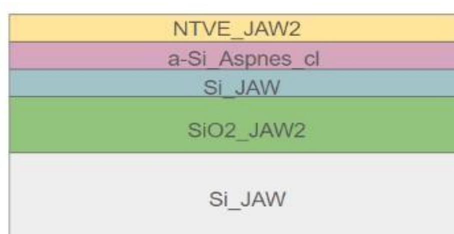

Figure 3.8: The Ellipsometry optical model consists of four layers on top of the Si substrate a SiO_2 layer (SIO2_JAW2), a crystalline Si layer (SI_JAW), an amorphous Si layer (a−Si_Aspnes_cl), and a native oxide layer on the top (NTVE_JAW2)

Once the preparation treatment is complete, the sample is placed in the chamber of the ICP-RIE tool to start the recipe and pump down to reduce the pressure as fast as possible to avoid any native oxide forming during the transfer between the preparation treatment and etching. After etching, the samples were measured by ellipsometry directly after processing to avoid any native oxide forming. The samples were then placed in a sample box inside a nitrogen box to prevent additional oxide formation during storage.

3.2.1 Reactive ion etching and ALE experiments

RIE sputtering and ALE experiments with ICP-RIE involving two recipes were decided for this project. First, a set of sputtering experiments was conducted to determine the influence of sputtering on the ALE process. The recipe for the sputtering experiment involves two steps, etching and purging, and can be visualised in Table 3.1. For sputtering, the tool's bias was changed from 10 to 300 V to find the sputtering threshold for Si and to compare it with the EPC of ALE.

Etching	Purge (1)
Cl_2 = 0 sccm	Cl_2 = 0 sccm
Ar= 10 sccm	*Ar*= 10 sccm
bias = 10-300 V	*bias* = 0 V
Temp = 20 C°	*Temp* = 20 C°
Time = 10 s	*Time* = 8 s
Pressure = 3 mTorr	*Pressure* = 3 mTorr
He pressure = 5 mTorr	*He* pressure = 5 mTorr
He flow = 6.15 sccm	*He* flow = 6.15 sccm

Table 3.1

The second set of experiments focused on ALE and was conducted accordingly. Four different sets of experiments were done with the aim of finding the "Q-ALE window." The first set involves increasing the bias of the tool from 10 to 150 V. The second set involves increasing the etch time from 10 to 45 s to prove that our process is in the ALE regime and optimise the recipe for the amount of gas used during processing. The third set of experiments will increase the number of cycles involving activation, purge (1), etching, and purge (2) from 25 to 100 cycles. By increasing the number of cycles, the etch depth will increase with the number of cycles, and so on, it will be easier to measure the etch depth and EPC, and more reliable results will be obtained by ellipsometry. This experiment will also show if the process will continue, based on increased cycles, as it should for ALE since it is a self-limiting etching process. By running the tool for longer, we will also get information on the tool's condition for an increasing number of cycles. The fourth set of experiments was to increase the pressure from 3 to 60 mTorr to improve the ALE process. An Al carrier was used for all the RFEA, sputtering, and ALE experiments. A Si carrier was also used to compare with the results from the Al carrier for higher cycle numbers and increased pressure experiments.

The ALE recipe differs from the sputtering recipe in several key steps. It includes an additional step called activation, which is crucial in the ALE process. This recipe also incorporates an extra purging step between activation and etching. Table 3.2 visually represents the ALE recipes for increasing bias, etch time, and number of cycles, highlighting these unique steps.

Activation	Purge (1)	Etching	Purge (2)
Cl_2 = 20 sccm	Cl_2 = 0 sccm	Cl_2 = 0 sccm	Cl_2 = 0 sccm
Ar= 0 sccm	Ar= 40 sccm	Ar= 10 sccm	Ar= 10 sccm
$bias$ = 0V	$bias$ = 0V	$bias$ = 10-150V	$bias$ = 0V
$Temp$ = 20 C°	$Temp$ = 20 C°	$Temp$ = 20 C°	$Temp$ = 20 C°
$Time$ = 20 s	$Time$ = 60 s	$Time$ = 10-45 s	$Time$ = 8 s
$Pressure$ = 30 mTorr	$Pressure$ = 3/60 mTorr	$Pressure$ = 3/60 mTorr	$Pressure$ = 3 mTorr
He pressure = 5 mTorr	He pressure = 5 mTorr	He pressure = 5 mTorr	He pressure = 5 mTorr
He flow = 6.15 sccm	He flow = 6.15 sccm	He flow = 6.15 sccm	He flow = 6.15 sccm

Table 3.2

The recipes for ALE and sputtering have been developed using results from previous experiments.[21][5] In the same way, as for the sputtering, the supplied energy will be in terms of bias. The bias is unique for the ICP-RIE tool, but it can be converted to RF power by the tool itself and ion energy by RFEA measurements, which will be used in this project. For this project, we decided to use the highest intensity ion energy peak from the IEDF curves as a reference value for comparing the RFEA measurement with etching experiments. This decision was made for the sake of simplicity when plotting the EPC and etch depth. Although IEDF is not a precisely defined value, the ion energy peak is where most ion energy density is concentrated, meaning that most ions have this energy.

3.2.1 Surface damage evaluation by EDS and AFM

The etched samples were analysed by SEM, EDS, and AFM to characterise surface roughness. The samples that were characterised were for three different types of experiments involving these surface characterisation techniques. First, AFM was done for ALE experiments, Table 4.1, with increasing bias and SEM images. SOI samples used for AFM were from the previous set of samples. Second, EDS was done with an increased number of cycles and increasing pressure with Al and Si carriers. For EDS, we etched new samples under the same condition as previously so as not to be affected by contamination during storage. Third, we performed EDS on two substrates, a Si and a GaAs sample, using 40 V and 60 mTorr for 25 cycles with a Si carrier. The samples were etched on the same carrier with a 2 cm distance between them for this experiment. This was done to compare the two samples under identical conditions for EDS analysis. A reference sample was also taken to EDS for each sample to compare the elemental composition of an unetched sample with an etched sample. EDS was used with the accelerating voltage of 10 and 5 kV, corresponding to the electron interaction depth of 1μm with a radius of 0.6 and 0.3 μm with a radius of 0.2 μm, respectively. The EDS system used in this project was a QUANTAX FlatQUAD from BRUKER.

Chapter 4

Result and Discussion

4.1 RFEA measurements of Ar+ ion energy and flux

This project aimed to investigate the consequences of plasma-assisted Q-ALE on damage and surface effects in Si. Specifically, the project aims to evaluate how Si is affected by a low-energy Q-ALE. This section presents the results of Q-ALE induced surface damage of the etched Si. To achieve this, we first needed to characterise the plasma discharge to understand the Ar+ ion energy distribution in the low-energy region of our Q-ALE process. In-situ RFEA measurements were conducted by measuring the IEDF of Ar+ ions at different ICP-RIE conditions (e.g., RF-power, pressure, etc.) to correlate the ion energy with the measured extent of the Si damage for the ICP-RIE tool that is used for the Q-ALE process.

Figure 4.1 shows the IEDF of Ar+ ions in plasma for different values of RF-excitation power, ranging from 1-6 to 28-32 W, corresponding to voltage setpoints of 7 to 120 V. The operating pressure was kept constant at 3 mTorr. The IEDF curves in Figure 4.1 show two ion energy distribution peaks: the main peak at high energy, ranging from 40 to 150 eV, and another peak below 20 eV. Increasing the RF-excitation power (voltage setpoint) shifts the Ar+ energy to higher values for both peaks. Simultaneously, the main peak broadens as the power increases. The position of the main peak at low power levels is around 50 eV, which is close to the Ar+ ion sputtering threshold of chlorinated Si (40 to 60 eV), according to the experimental data.[12][4][13]

Figure 4.2 illustrates how IEDF changes with gas pressure, ranging from 3 to 60 mTorr at a fixed power of 7-17 W corresponding to the voltage setpoint of 40 V. The graph in Figure 4.2 shows that the ion energy decreases as the pressure increases. The peak ion energy decreases from around 70 eV at 3 mTorr to 10 eV at 60 mTorr. However, it is worth noticing that the ion energy distribution width also increases with the pressure. This means that by increasing the pressure, one can achieve lower ion energies, but at the same time, the wider ion energy distribution results in a high-energy tail (up to 100 eV). One explanation for the low energy peak at high pressure could be attributed to the loss of ion energy due to more frequent collisions of ions with the gas molecules.

However, for low ion energy at 0 to 10 eV, we can see that a low-energy peak of around 10 eV is beginning to form; this low-energy peak was also present for the RFEA experiment with increasing bias but not as prominent as for increasing pressure. This low-energy peak is getting broader as the pressure increases, and at

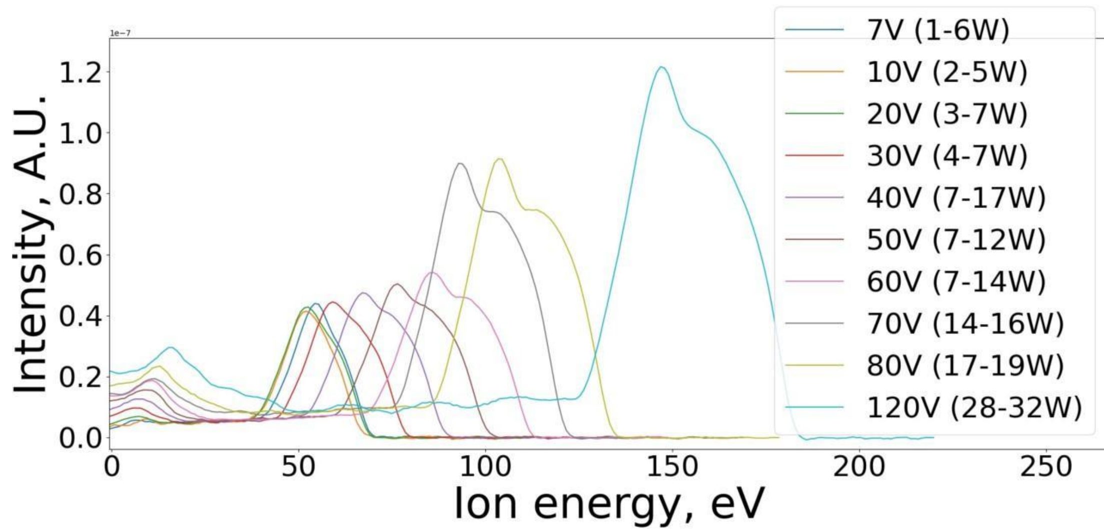

Figure 4.1: Ar+ plasma ion energy distribution function (IEDF) for the DC bias-setpoint for 7, 10, 20, 30, 50, 60, 70, 80, and 120 V of RF plasma. All experiments were conducted at 3 mTorr.

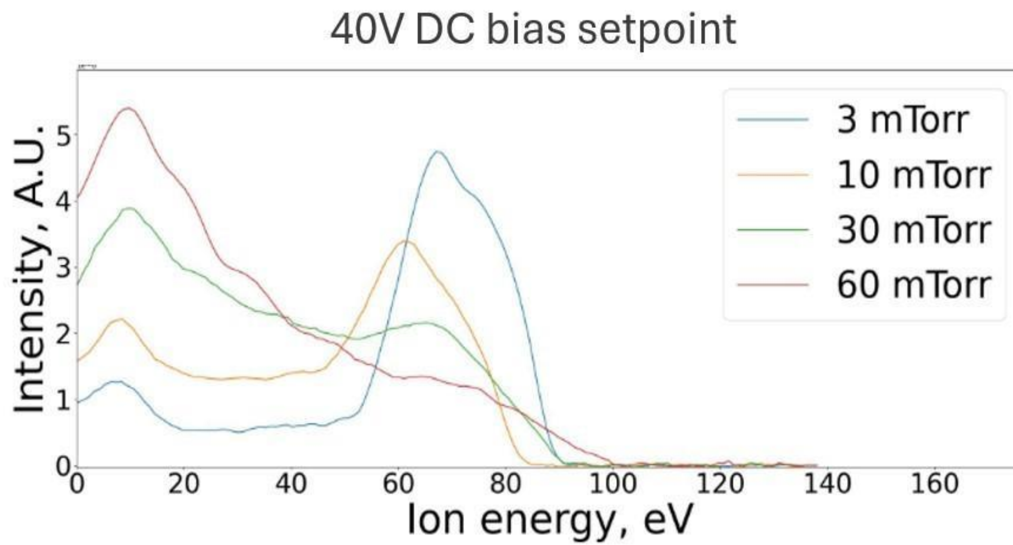

Figure 4.2: Ar+ plasma ion energy distribution function (IEDF) for pressure for 3, 10, 30, 60 mTorr and for 40 V bias

30 mTorr, the average ion energy is shifted towards this low-energy peak. This means that most of the ions are falling within this ion energy range. However, it is known that IEDF peaks close to 0 eV are expected at higher pressure since the higher the pressure, the more collisions are expected between ions and molecules in the plasma. As ions collide with molecules, they will lose energy, resulting in a low-energy peak detected during RFEA measurement. The higher the pressure, the more dominant this low-energy peak becomes as the mean free path of the ions decreases. This suggests that low ion energy peaks at approximately 10 eV and below arise from collisions of ions in the plasma and not contribute to the Q-ALE [31]. However, this area requires further investigation, as the potential presence of low-energy ions is intriguing and could benefit our Q-ALE process. For instance, at 60 mTorr, we have observed a single ion energy peak at around 10 eV. This is promising when studying damage-free ALE since the contribution of high-energy ions will not be as prominent as that of low pressure. However, for this project, it was decided to proceed with a pressure of 3 mTorr to understand better the ions used in the etching process. It was decided to investigate the influence of a higher pressure of 60 mTorr to explore the possibility of achieving etching with low-energy ions. To simplify data analysis, it was decided to use the values of the peak energy and the average energy calculated over the whole energy range.

Figures 4.3 and 4.4 plotted the peak and average ion energy from RFEA measurements as a function of bias and pressure, respectively. The data in Figure 4.3 were obtained at the pressure of 3 mTorr. The ion flux of the Ar+ ions was also calculated from the RFEA data and is shown in Figures 4.5 and 4.6. The ion flux was measured as a function of power (bias setpoint) and pressure. An increase in RF power leads to higher plasma density (or ion flux). Since the ion flux is proportional to the increase in RF power, we can infer that the number of ions hitting the surface of the material etched per unit area per unit time increases. The higher ion flux typically leads to a higher etch rate because more ions are available to physically sputter and chemically react with the surface material. However, we can see that the increase in ion flux is not proportional to the increase in RF power below 5 W or 20 V bias.

This is probably because the power level required to initiate and sustain the plasma is too low. If the power supplied is too low, the plasma will not be fully ignited or stable, leading to an insufficient ionisation rate. The pressure dependence in Figure 4.2 is that plasma density increases with pressure due to a higher concentration of molecules. During ionisation events in the plasma, this results in a higher ion and electron concentration and, thus, a higher current and ion flux. The ion flux for the ICP-RIE system used in this project is similar to values found in other studies [12][4][13]. This indicates that the properties, such as ion current density or ion flux required for the ALE process used in this project, are consistent with those of similar studied systems and comparable in terms of etching parameters. The ion energy and ion flux are crucial factors in etching processes. Therefore, the RFEA information about the ICP-RIE system is helpful for comparing actual experiments with molecular dynamic simulations, where the ion energy and ion flux are the primary input parameters.

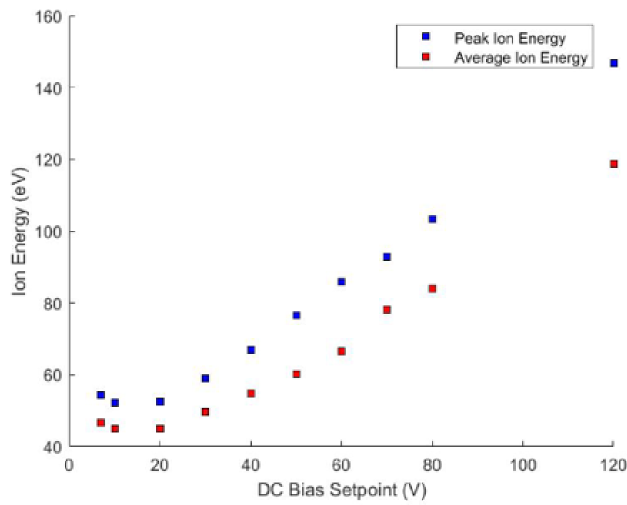

Figure 4.3: Peak and average ion energy from RFEA measurements as a function of DC bias setpoint (V)

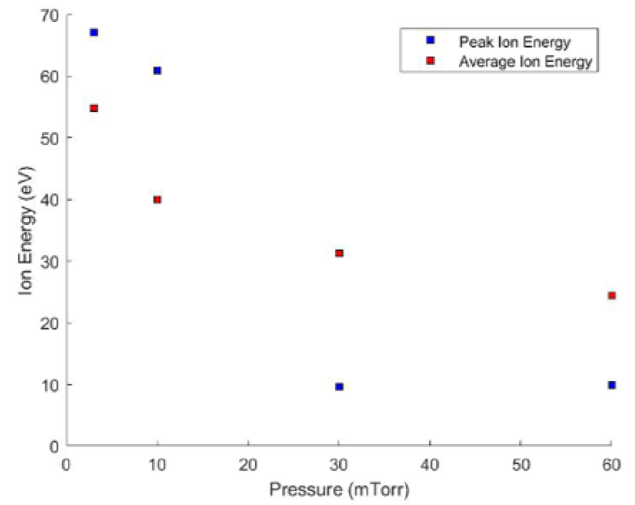

Figure 4.4: Peak and average ion energy from RFEA measurements as a function of pressure (mTorr) for 40 V bias

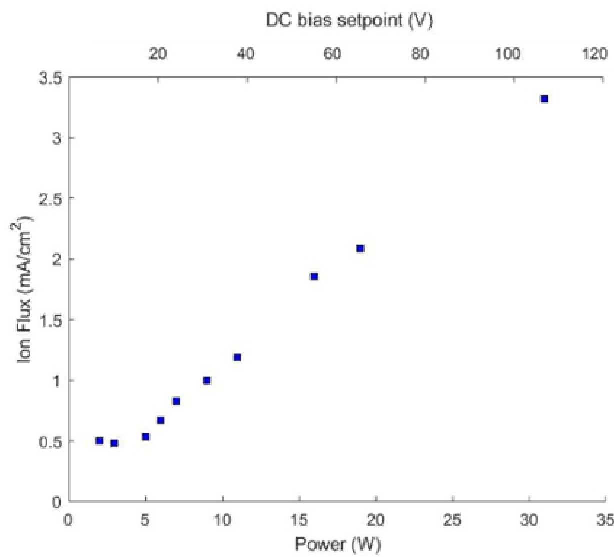

Figure 4.5: Ion flux of the Ar+ ions form the RFEA data as a function of power (W) and DC bias setpoint (V) in the second x-axis

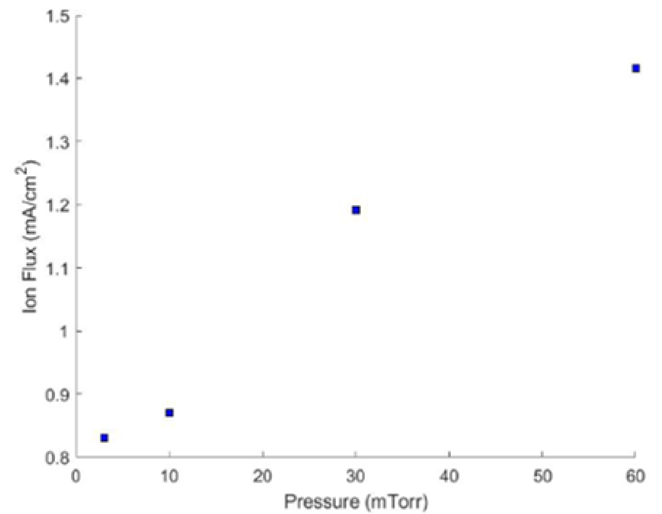

Figure 4.6: Ion flux of the Ar+ ions form the RFEA data as a function of pressure (mTorr) for 40 V bias

4.2 Etch Per Cycle Analysis: Effects of Bias, Bombardment time, and number of Cycles

After characterising the Ar+ ions from the RF-plasma discharge, sputtering and Q-ALE experiments were conducted according to the respective recipes in Tables 3.1 and 3.2. Performing a synergy test in an ALE process is crucial for detecting unwanted etching caused by high-energy ions, which can physically dislodge Si atoms from the surface. This test helps ensure process selectivity by identifying and quantifying unintended etching and optimising ion energy levels to prevent physical sputtering while maintaining the desired chemical reactions.

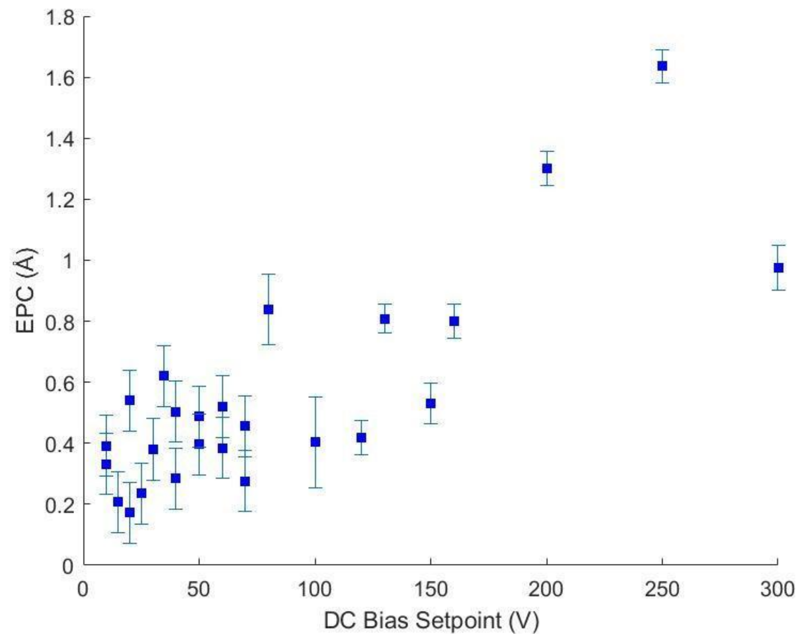

Figure 4.7: Sputtering experiment for 10 to 300 V DC bias setpoint voltage, and EPC (Å)

Figure 4.7 presents the results of the sputtering experiments (parameters are in Table 3.1), showing EPC as a function of bias. All experiments were performed under 10 s etch duration at 3 mTorr operating pressure for 25 cycles. After each experiment, ellipsometry was used to determine the amount of etch. According to Figure 4.7, the EPC increases from 0.2 to 1.6 Å as the bias was increased to 300 V. For energies corresponding to approximately 100 V bias, the result shows very scattered data ranging from 0.2 up to 0.8 Å, and the EPC does not appear to be significantly affected by an increasing bias. However, above 100 V, there is a clear increase in the EPC. It may be that the RF discharge is not stable enough at low energies, or the process is close to or under the sputtering threshold. An unstable RF discharge would lead to a non-linear relationship between the applied RF power and ion energy, especially at bias values below 30 V. This is visible in Figure 4.3, as the peak ion energy does not start to increase continuously until approximately 50 eV

(20 V bias). Another explanation is that the relative inaccuracies of ellipsometry measurements increase at small etch depths. This could mean that the scattered data in Figure 4.7 might be due to inaccuracies in the ellipsometry model. Since the amount of etch is very low, errors in the ellipsometry model could lead to the observed scattered data. The accuracy of the thickness measurements is thus one of the key considerations here.

However, from Figure 4.7, one can see that a continuous increase in EPC is proportional to increasing bias starting at 60 to 100 V bias (50 to 70 eV, converted into peak ion energy). This is an expected and well-studied process since it is above the sputtering threshold of Si [12][4][13][14], where enough excess energy is supplied to break the bonds of the Si atoms of the outermost surface. It is also worth mentioning that the EPC also seems to decrease for higher energies above 146 eV (250 V bias). However, this energy range is far beyond the ion energy region of interest for ALE. Since this observation was based on a single set of measurements and it's generally expected that the sputtering rate should increase with ion energy, this data point was considered an outlier.

The sputtering effect can damage the surface, making detecting uniform and continuous etching challenging for the ellipsometry measurement. Sputtering can use any ion energy as long as it is enough to break the bonds of the target atoms and remove them from the surface.[9][10][11]. However, higher energies can affect the surface and the atoms beneath it.

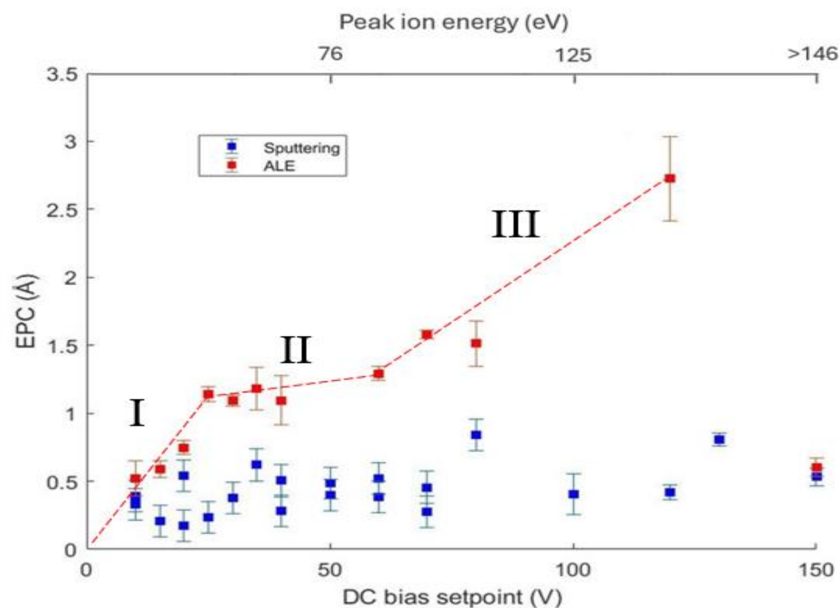

Figure 4.8: Q-ALE and sputtering experiment up to 150 V bias corresponding to 146 eV peak ion energy according to RFEA in figure 4.1 and EPC (Å)

The results of the plasma-assisted Q-ALE experiments conducted as per the recipe in Table 3.2 are shown in Figure 4.8 and the sputtering experiment from Figure 4.7. In Figure 4.8, the EPC is plotted as a function of bias setpoint with corresponding Ar+ peak energy position in the second x-axis. In the ALE experiments represented by the red dots, three distinct regions can be observed:

I) Region I (7 to 25 V): There is a steep increase in EPC. We attribute this region to incomplete ALE, where the process has not stabilised.

II) Region II (25 to 60 V): The EPC increases slowly and appears almost independent of the applied bias. This region is characterised as quasi-ALE (Q-ALE), indicating a more stable and controlled etching process.

III) Region III (60 V and onward): The EPC increases proportionally to the applied bias. In this region, the sputtering contribution becomes significant, indicating that the process has moved beyond the Q-ALE mode.

These observations suggest that below 25 V, the ALE process is incomplete; between 25 and 60 V, a stable quasi-ALE process is achieved, and above 60 V, sputtering effects dominate, altering the etching dynamics.

This EPC value in the range of 25 to 60V (Region II) is close to the expected range for ALE of Si (100) monolayer, based on the theoretical thickness of 1.36 Å.[17][18] In an ideal scenario, only one monolayer of material should be etched in each ALE cycle. However, due to the contribution from the physical sputtering of Si by Ar plasma, the EPC is not entirely constant in the range of 25 to 60 eV, showing a gradual increase. This is why we attribute this region to quasi-ALE. This ALE process falls within this range, indicating that this region is within the self-limiting ALE window.[9][10][11] However, molecular simulation suggests that the energy threshold for the ALE to occur can be as low as 20 eV. Experimental studies, on the other hand, show that for Si to desorb after activation, it requires at least 50 eV of ion energy.[9][10][11] According to our experimental results from Figure 4.8, it can be concluded that ALE is not achieved in the low-energy region at 20 eV as predicted by molecular simulation in the references.[9][10][11] Still, in the region of about 50 eV Ar+ energy, ALE is taking place in experimental results.[9][10][11] When comparing sputtering (blue dots) and Q-ALE experiments (red dots) in Figure 4.8, it is evident that the Q-ALE process has a significantly higher etching rate than the sputtering process described in Table 3.1. The difference in EPC between sputtering and Q-ALE increases from approximately 0.6 to 2 Å as the bias increases. The high etch rate for Q-ALE is due to the interaction of Cl gas with Si atoms, which loosens the Si atoms. Subsequent bombardment of these loosened atoms with low-energy Ar ions results in their removal, a process that does not occur in sputtering experiments without Cl gas injection.

Experiments were conducted to optimise the Q-ALE recipe by increasing the etch time and the number of cycles. A perfect ALE should be independent of the duration of the etch step; in a Q-ALE, the increase in etch time will result in an increase in EPC. Variation in a number of cycles will not affect the EPC in the case of a perfect ALE. For the

experiment, the same recipe as before in Table 3.2 was followed for two different biases, 25 and 40 V, corresponding to Ar+ peak ion energy of 57 and 67 eV. Both biases are within what is believed to be the self-limiting Q-ALE window, as shown in Figure 4.8. In Figure 4.9, the EPC is plotted as a function of etch time for different peak ion energy 57 eV (25 V bias) in blue and peak ion energy 67 eV (40 V bias) in red. For 25 eV, the etch time varied from 10 to 30 s; in this period, the EPC increased with etch time, indicating non-ideal ALE. Ideally, in an ALE process, increasing the etch time does not change the etch per cycle (EPC) because the process is self-limiting. In each cycle of ALE, the material removal is controlled by sequential, self-limiting surface reactions. This means that once a monolayer of material is prepared and etched away, additional exposure time does not result in further etching beyond this monolayer. The etching stops automatically after removing the desired layer thickness, ensuring precise and consistent material removal regardless of the etch time.

However, since the etching process involves plasma-assisted Q-ALE, the behaviour is not entirely self-limiting with increasing etch time. This is because some etching still occurs due to sputtering. As mentioned earlier, sputtering can use any ion energy as long as it is enough to break the bonds of the target atoms and remove them from the surface. Adsorbing Cl_2 gas on the Si surface will tremendously increase the sputtering rate by so-called reactive sputtering.

For the peak Ar energy of 67 eV (40 V bias), the EPC increases with etch time duration up to 25 s. For longer etch times, the EPC decreases just above 0 Å. According to the literature review, one would expect similar behaviour for 67 and 57 eV since both are either in or just above the ALE regime, according to Figure 4.8. It is possible that 67 eV falls outside of the Q-ALE regime and instead is affected by RIE sputtering to a larger extent, leading to a different behaviour than is the case for 57 eV peak ion energy, causing damage. Based on Figure 4.9, if the etching step in the ALE recipe runs for more than 35 s during the etching step, it appears that there will be no etching or that we deposit material at the same rate as we etch it. This could be due to surface damage or insufficient etching causing redeposition. Suppose the etching is running for a long period of time, and the etched material does not get purged out. In that case, there is a probability that this material will be redeposited on the surface, as discussed for surface damage in the theoretical background. If we etch as much as is redeposited, the EPC will be kept unchanged. However, to optimise the recipe, we should keep the etch time below 25 s to prevent a decrease of the etch rate of the process with 57 eV and 67 eV peak ion energy.

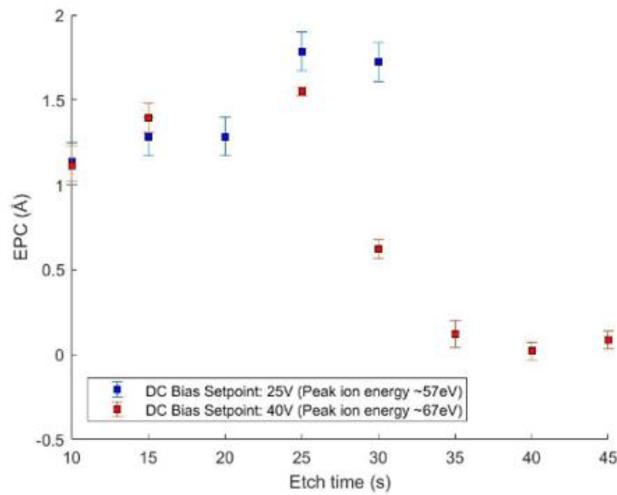

Figure 4.9: ALE etch time experiment for 10, 15, 20, 25, 30, 40 and 45 s, and EPC (Å) for bias 25 V and 40 V or 57 eV and 67 eV peak ion energy

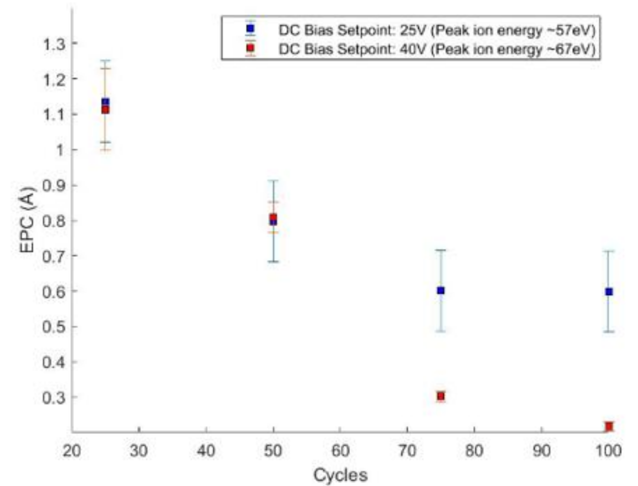

Figure 4.10: ALE cycles experiment for 25, 50, 75 and 100 cycles, and EPC (Å) for bias 25 V and 40 V or 57 eV and 67 eV peak ion energy

In Figure 4.10, the ALE experiment for increasing the number of cycles is shown. In Figure 4.10 we are comparing the results of EPC by the number of cycles as for the etch time experiments for peak ion energy 57 eV (25 V bias) in blue and peak ion energy 67 eV (40 V bias) in red. The EPC decreases with increasing cycles, but for the peak ion energy 57 eV, the EPC is approximately 0.4 Å lower for 75 and 100 cycles than for the peak ion energy 67 eV. In the ideal case, the EPC should not be affected by the number of cycles, but as we can see from Figure 4.10, this is not the case. As for the etch time experiment, the EPC decreases.

It seems that to increase the etch time and the number of cycles, we observe a stop in the etching, which we attribute to the redeposition of the etched components at the same rate as we etch them. A possible model of the surface process includes two contributions: (1) etching, including its sputtering component and (2) redeposition of the etched material. The etching and deposition compete with each other, and at a small number of cycles, etching dominates, while at a large number of cycles, the deposition takes over. The reasons for such behaviour are not really understood, but the experimental ellipsometric data (below) support this hypothesis. Since the main purpose of this project is to evaluate the damage induced by ALE, we conducted our damage-related experiments with 10 s etch time and 25 cycles to ensure consistent and reliable results.

After conducting the Q-ALE experiments above, it was concluded that the ALE characteristic behaviour was achieved with a 10 s etch time and 25 cycles, resulting in close to one monolayer of Si etched per cycle. Therefore, it was decided to move forward with surface damage evaluation according to these parameters since this is believed to be the closest to what we want to achieve by our Q-ALE process. Ideally, the real ALE process should be independent of both etching time and the number of cycles. However, the obtained results suggest that this is not completely the case when the

etching is going on for a longer period of time, whether it is due to longer etching time or longer processing of a number of cycles. To further evaluate what could be the source of this decrease in etching rate, we decided to study the etch depth of the individual single layer using an ellipsometry optical model.

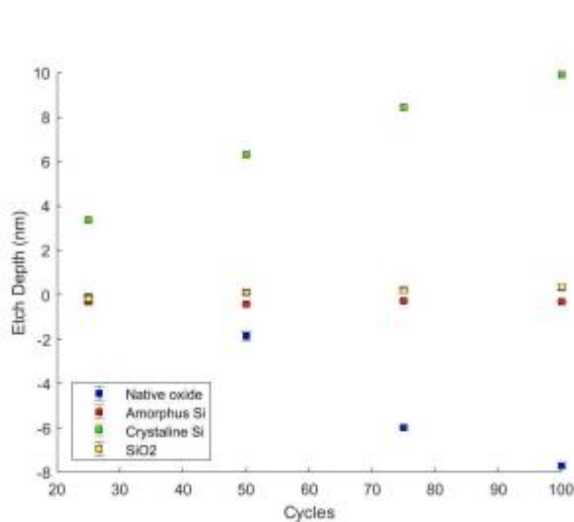

Figure 4.11: ALE with increasing number of cycles experiment vs etch depth (nm) of individual layers of ellipsometry optical model SiO_2 layer (SIO2_JAW2, in yellow), crystalline Si layer (SI_jAW, in green), amorphous Si layer (a–Si_Aspnes_cl, in red), and the native oxide layer (NTVE_JAW2, in blue)

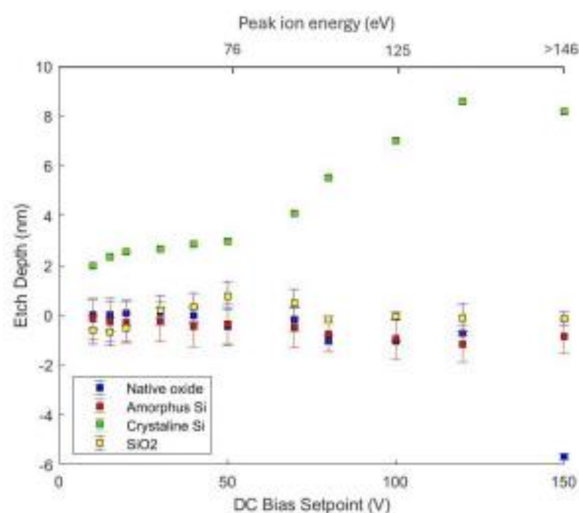

Figure 4.12: ALE with increasing bias experiment vs etch depth (nm) of individual layers of ellipsometry optical model SiO_2 layer (SIO2_JAW2, in yellow), crystalline Si layer (SI_jAW, in green), amorphous Si layer (a–Si_Aspnes_cl, in red), and the native oxide layer (NTVE_JAW2, in blue)

4.3 Ellipsometry Analysis of the Layers Thickness

A change of thickness of different layers for the SiO_2 layer ($SIO2_JAW2$, in yellow), crystalline Si layer (SI_jAW, in green), amorphous Si layer (a –Si_Aspnes_cl, in red), and the native oxide layer ($NTVE_JAW2$, in blue) according to the ellipsometry optical model, are shown in Figure 4.11 and 4.12. The figure shows the variation in etch depth as a function of bias and the corresponding peak ion energy in the second x-axis and the number of cycles in Figure 4.12, respectively. From Figures 4.11 and 4.12, we will identify the material that has been etched and detect any changes in etch depth between different layers, which could influence the etching rate as the number of cycles and bias increase.

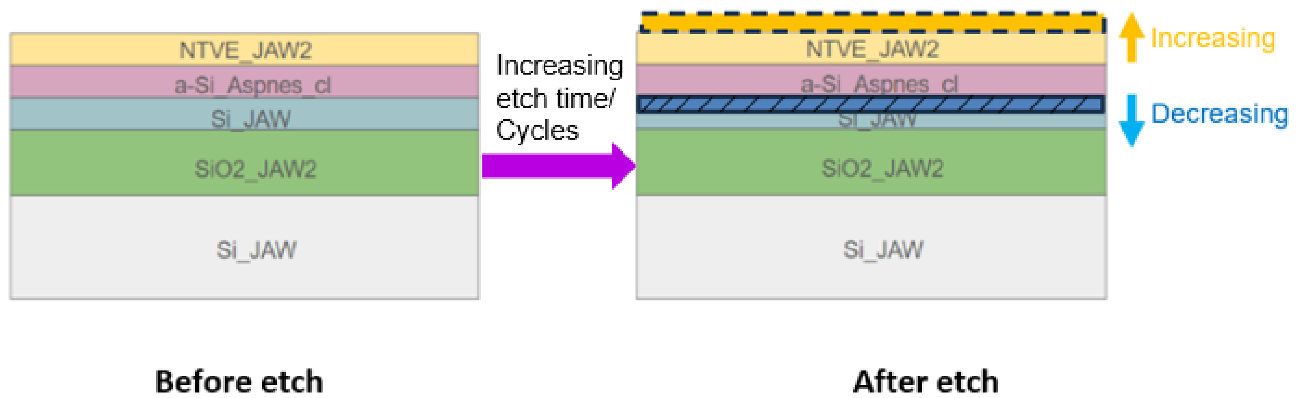

Figure 4.13: Ellipsometry optical model after etching by increasing number of cycles and bias. The model consists of four layers on top of the Si substrate: a SiO_2 layer (SIO2_JAW2), a second crystalline Si layer (SI_JAW), an amorphous Si layer (a – Si_Aspnes_cl), and a native oxide layer (NTVE_JAW2

Figure 4.11 shows that the amorphous Si and SiO2 layer etch rates are kept unchanged, independent of the increasing bias or number of cycles. The SiO_2 layer is not affected by the etching. This is expected since the SOI samples have a 60 nm thick Si layer on top of the SiO_2, and the etching depth is only 10 nm for 100 cycles, according to Figure 4.11. Ar+ ions with energies ranging from 50 to 150 eV cannot penetrate the 60 nm thick Si layer to reach the underlying SiO2 layer. The amorphous Si layer represents the damaged layer after etching and does not seem to be affected by increasing the bias or the number of cycles, according to ellipsometry data. However, both are kept unchanged and have a thickness change of less than 1 nm, making only a negligible contribution to the total etch depth. It is interesting to note that when comparing the individual layers of the ellipsometry optical model, most of the total etch depth comes from the native oxide and crystalline Si layers for both increasing bias and number of cycles. For the native oxide, the etch depth decreases with increasing cycles and bias. Meanwhile, for the crystalline Si, the etch depth increases for an increasing number of cycles. The decrease in crystalline Si is expected since this is the layer that we want to etch with the Q-ALE process. However, the decrease in etch depth for the native oxide means that we grow a native oxide layer on top of the SOI structure, which is problematic. It has previously been noted that the native oxide forming on the SOI samples will form rapidly due to the highly reactive surface of Si after etching. However, the thickness of the native oxide should be relatively consistent and should not increase with increasing bias or the number of cycles. In addition, the SOI sample was measured by ellipsometry as fast as possible after etching to avoid forming the native oxide. It is reasonable to assume that something other than oxygen and forming a native oxide layer contributes to the big difference in etch depth for increasing bias and pressure according to the optical model that ellipsometry refers to.

Consequently, the formation of native oxide appears to result from the decreased etch rate. This suggests that changes occur on the surface of the SOI sample during extended etching periods, as previously concluded with increasing etch time and number of cycles. Surface damage occurs due to sputtering by ions, as described as consequences when using plasma-enhanced Q-ALE. Damage to the surface can affect the optical density at the interface and the fitting of the optical model, leading to an incorrect estimate of the single-layer thickness. Ellipsometry was used to obtain information about the etched thickness, but it cannot provide details about the elemental composition or damage evaluation of the materials. Therefore, we conducted an EDS and AFM investigation to analyse the formation of the native oxide layer referred to in the ellipsometry optical model.

4.4 Surface damage evaluation by EDS and AFM

Figure 4.14 a) shows the EDS spectra and the corresponding SEM images for a new set of SOI samples etched with 79 eV peak ion energy (40 V bias) according to the recipe in Table 3.2 for 25, 50, 75, and 100 cycles. Upon first examination of the SEM images, they clearly show the formation of island-like structures on the Si surface already at 25 cycles. The island-like pattern becomes more pronounced as the number of cycles increases, forming larger island coalescence structures. As the number of cycles increases, surface island formation gives rise to island coalescence structures that almost completely cover the surface for 75 and 100 cycles. Island formation on the surface can be attributed to sputtering or other sources and will require further evaluation.

The EDS spectra in figure 4.14 b) reveal the elemental composition of the etched surface, indicating the presence of silicon (Si), aluminium (Al), and tin (Sn). The EDS spectra detected carbon (C) and oxygen (O) with signal peaks below 1 keV, which is considered below the reliable resolution for quantification of the EDS tool. In the EDS analysis, it is common to detect C and O, as those elements are very abundant. However, they likely appear as characteristic X-rays originating from either the system or the sample holder or due to contamination or formation of native oxide on the sample.

25 Cycles

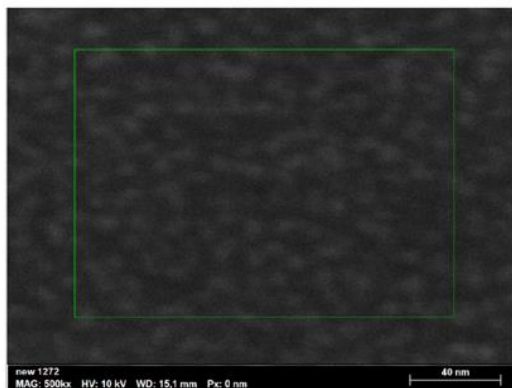

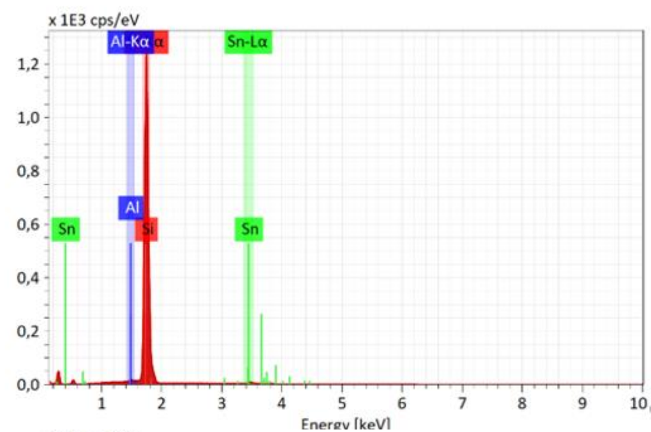

50 Cycles

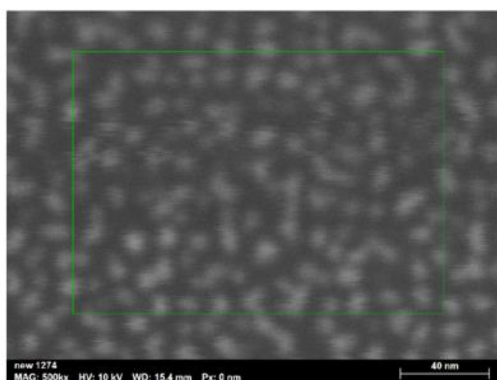

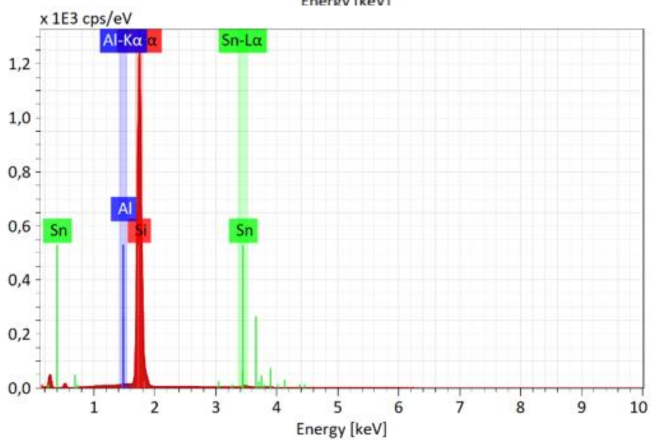

75 Cycles

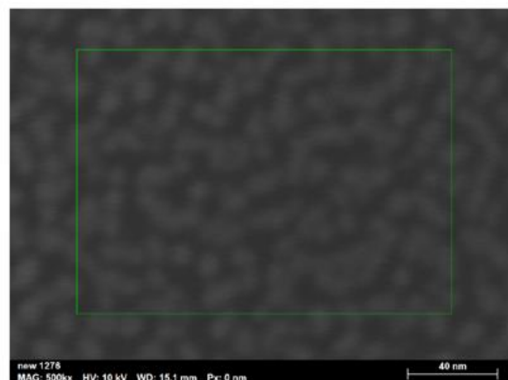

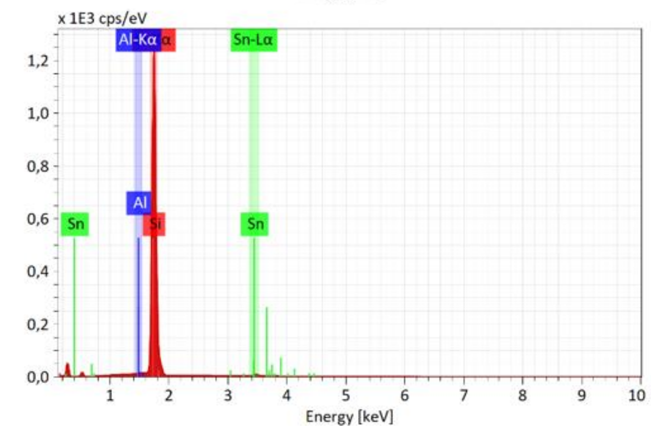

100 Cycles

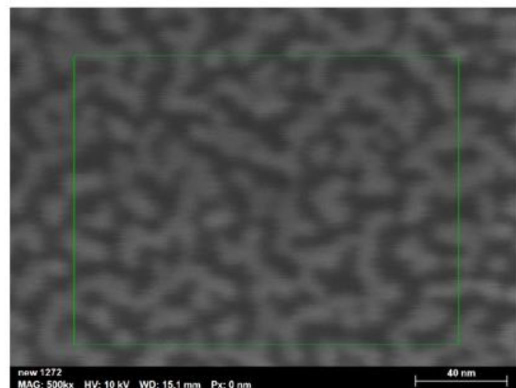

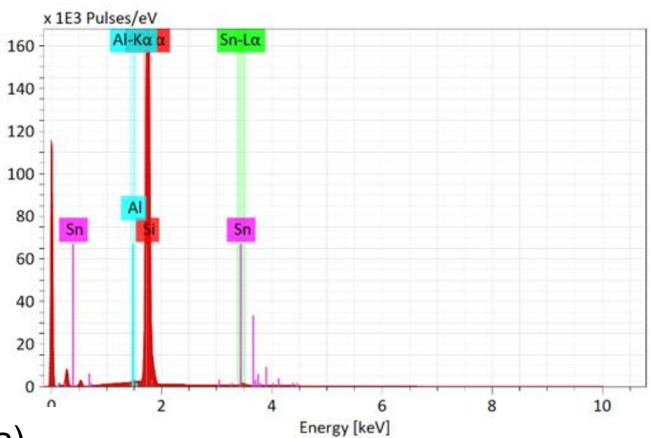

a)

Map

25 Cycles

Element	At. No.	Net	Mass [%]	Mass Norm. [%]	Atom [%]	abs. error [mass%] (1 σ)	rel. error [%] (1 σ)
Silicon	14	14511773	163,65	98,07	98,45	3,87	2,37
Aluminium	13	179563	2,26	1,35	1,41	0,07	2,96
Tin	50	69327	0,96	0,58	0,14	0,02	2,23
		Sum	**166,87**	**100,00**	**100,00**		

50 Cycles

Element	At. No.	Net	Mass [%]	Mass Norm. [%]	Atom [%]	abs. error [mass%] (1 σ)	rel. error [%] (1 σ)
Silicon	14	12129987	162,51	98,19	98,58	3,89	2,39
Aluminium	13	135133	2,02	1,22	1,27	0,06	3,02
Tin	50	59593	0,98	0,59	0,14	0,02	2,30
		Sum	**165,51**	**100,00**	**100,00**		

75 Cycles

Element	At. No.	Net	Mass [%]	Mass Norm. [%]	Atom [%]	abs. error [mass%] (1 σ)	rel. error [%] (1 σ)
Silicon	14	13181856	163,01	98,18	98,56	3,88	2,38
Aluminium	13	149645	2,06	1,24	1,30	0,06	2,99
Tin	50	63151	0,97	0,58	0,14	0,02	2,28
		Sum	**166,04**	**100,00**	**100,00**		

100 Cycles

Element	At. No.	Net	Mass [%]	Mass Norm. [%]	Atom [%]	abs. error [mass%] (1 σ)	rel. error [%] (1 σ)
Silicon	14	16398218	163,93	98,16	98,53	3,85	2,35
Aluminium	13	192068	2,14	1,28	1,34	0,06	2,94
Tin	50	74958	0,93	0,56	0,13	0,02	2,21
		Sum	**167,00**	**100,00**	**100,00**		

b)

Figure 4.14: a) EDS spectrum for a set of SOI samples etched with 40 V bias (79 eV peak ion energy) according to the recipe in Table 3.2 with the increasing number of cycles with belonging high-resolution SEM images, at 10 kV accelerating voltage, MAG 500kX. b) table of quantitative elemental analysis from EDS spectrum. From EDS analysis, it was not possible to distinguish the elemental composition of the island-like structures*.*

When looking into the EDS spectra with energy above 1 keV, one can see that Si, Sn and Al are present. From the quantification of the EDS spectrum, one can see that the mass (%) and atom (%) of Al and Sn are independent of a number of cycles, suggesting that these may be artefacts peaks from within the system. Sn is known to be very aggressive when exposed to plasma etching. An etching or sputtering of Sn will lead to its re-deposition on the inner chamber walls and substrates, so some traces of Sn can be found everywhere, including the substrate surface.[43] However, in our case, we were unaware of any use of Sn, and the amount of Sn in the ICP-RIE system appears much less than expected, suggesting that this be an artefact peak resulting from the software quantification of the EDS spectrum. After examining the energy tables [44], it was discovered that Sn has an M-peak at 0.691 keV, which does not match the observed EDS spectrum.

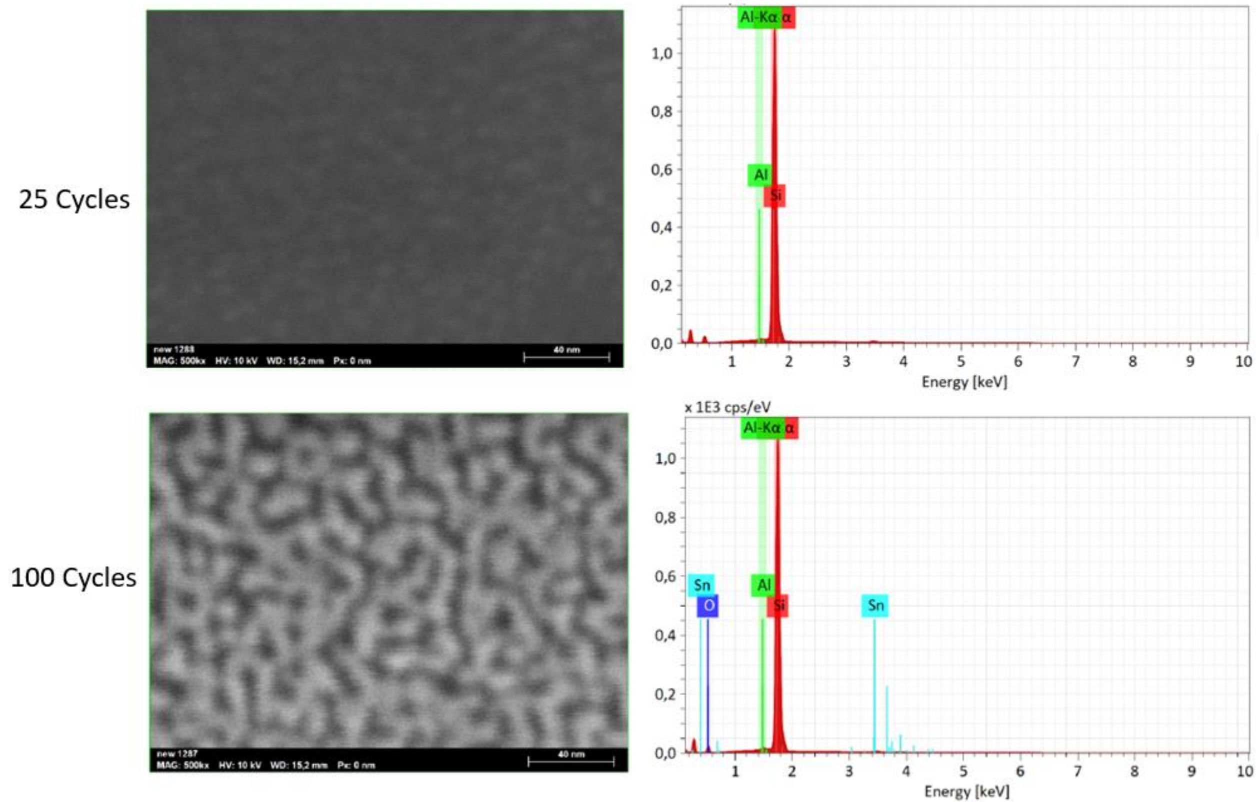

a)

Map

25 Cycles

Element	At. No.	Net	Mass [%]	Mass Norm. [%]	Atom [%]	abs. error [mass%] (1 σ)	rel. error [%] (1 σ)
Silicon	14	12062849	85,08	99,63	99,61	1,95	2,29
Aluminium	13	62582	0,32	0,37	0,39	0,01	3,25
		Sum	**85,40**	**100,00**	**100,00**		

100 Cycles

Element	At. No.	Net	Mass [%]	Mass Norm. [%]	Atom [%]	abs. error [mass%] (1 σ)	rel. error [%] (1 σ)
Silicon	14	11785579	116,46	98,44	98,38	2,72	2,33
Aluminium	13	167798	1,84	1,56	1,62	0,05	2,91
		Sum	**118,31**	**100,00**	**100,00**		

b)

Figure 4.15: a) SEM image, 10 kV accelerating voltage, MAG 500kX. EDS spectrum of Q-ALE experiment according to Table 3.2 for 3 mTorr pressure, 25 cycles and 100 cycles with Si carrier. b) table of quantitative elemental analysis from EDS spectrum. From EDS analysis, it was not possible to distinguish the elemental composition of the island-like structures*.*

It was concluded that the EDS signals originally attributed to Sn were an artefact and that we did not expect any Sn in the tool. It is more reasonable to expect the presence of Al in the EDS spectrum since Al was used as the carrier during Q-ALE. Al may be etched to a small extent along with Si during the process if a large surface is exposed. However, whether the Al atoms possess sufficient energy to transfer and deposit onto the SOI sample is still unclear. To determine whether the Al peaks are artefacts from the system, we conducted one extended set of Q-ALE experiments using the same parameters and conditions as before but with a Si carrier instead of an Al carrier. This will help us

conclude whether the EDS spectrum depends on the carrier and whether the Al originates from the carrier or the plasma chamber.

Figure 4.15 a) and b) shows the EDS spectrum under the same conditions as previous experiments for 25 and 100 cycles, using a Si carrier instead of an Al carrier. The SEM images show that the island surface island formation, as with the Al carrier, is still present and is increasing with the number of cycles. But the most noticeable thing is that even if we use a Si carrier, the EDS spectrum still shows traces of Al. It is also worth noticing that the content of Al by mass (%) and atom (%) is increasing with an increasing number of cycles, from 0.32 and 0.39 to 1.84 and 1.62%, respectively. Since the Al carrier is not used this time, the Al must come from another source within the RIE-ICP system, such as the chamber walls, unless it is an artefact. Since the EDS Al peak at 1.486 keV is very close to the Si peak at 1.739 keV according to energy tables [44], there is a possibility that the EDS software mistakes the Al peak to be an extension of the Si peak. Since neither Al or Si has β-, L- or M-peaks, it was decided to go for a different substrate with a different EDS peak further from the Al peak to be able to distinguish the Al peak. The substrate that was decided to be used instead of SOI was a GaAs sample with EDS peaks at 9.24 and 10.53 keV, according to the EDS energy tables.[44] When changing the sample, no Al peak was found, and it was concluded that the Al peak was most likely where an artefact peak generated by the software as an extension of the Si peak.

The SEM images indicate that the surface islands were still present even when a different carrier was used. Therefore, it was decided to process an additional SOI sample etched under the same condition as before but with increasing pressure during Q-ALE. Higher pressure will shift the Ar+ peak ion energy to lower values around 10 eV (Figure 4.2), thus minimising the sputtering effects. This will also make the Q-ALE process more isotropic and reduce the effect of directional etching, making the process gentler. The pressure was increased from 3 to 60 mTorr. This change was made because the IEDF from the RFEA measurement in Figure 4.2 showed that the ion energy for a 40 V bias was the lowest at 60 mTorr, with a peak energy of just 10 eV. This is in line with molecular simulations discussed in the theoretical background [12][4][13], which suggests that 20 eV is the lowest energy that can be used for ALE according to molecular simulation. However, the ion energy peak for 40 V bias at 60 mTorr is spread out over a large distribution up to 100 eV according to the RFEA measurement, so sputtering cannot be neglected entirely, even for higher pressure. However, the expectation is that the number of high-energy ions will be less than that of low-energy ions since the IEDF has its peak in the low-energy region. If most of the ion has low energy, this will reduce the effect of damaging the sample, which may be the source of the surface roughening and island formation visible in SEM. This will also indicate if the peak in IEDF at 60 mTorr from Figures 4.1 and 4.2 is real or if it is caused by collisions of ions in the plasma; it may not contribute to the Q-ALE. It was also decided to decrease the accelerating voltage from 10 to 5 kV to make the EDS spectra more surface sensitive since we are decreasing the interaction volume, improving the spatial resolution of the EDS analysis. Improving the spatial resolution will contribute to a more qualitative understanding of the composition of surface island formations.

Figures 4.16 and 4.17 show high-resolution SEM and respective EDS spectra for the reference and etched samples of GaAs and Si, respectively. It was decided to perform only 25 cycles of Q-ALE to be able to compare etched GaAs and Si with the reference samples. SEM images in Figure 4.16 show no surface roughening or island formation on the GaAs surface, unlike Si under the same conditions, Figure 4.17. This indicates that the surface island formation, presumably a deposition, is limited to the Si substrate. No EDS signals of Si were observed on the GaAs sample in Figure 4.16. So, it can also be concluded that since no traces of Si are detected on the GaAs surface, a possible redeposition of the etched material, e.g. Si, is taking place locally on the same surface, see SEM images in Figure 4.17. As seen in the SEM images, the island formation indicates a local re-deposition effect of Si. A comparison of SEM images in Figures 4.14 and 4.17 shows that the island formation on Si occurs even at a high pressure of 60 mTorr. Although the Ar+ ion energy is lower at 60 mTorr compared to 3 mTorr, the high-energy tail of 60-100 eV, seen in Figure 4.2, still contributes to the sputtering and re-deposition of Si, resulting in the island deposition.

The SEM images indicate that the surface deposition effect of the islands increases with the number of cycles, forming larger island formation coalescence structures. This explains why there is a significant decrease in EPC for increasing etch time and number of cycles. Figures 4.9 and 4.10 clearly illustrate this. The ellipsometry measurements give averaged values over a large area, a millimetre or so in our case. Hence, the growth of island layers does not significantly affect ellipsometry measurements when the islands occupy only a small portion of the total measured area. However, as the islands coalesce, the deposited material covers a more significant part of the probed area, eventually encompassing most of the surface. This affects the measurement of EPC, as the ellipsometer will then measure it as a continuous surface, requiring corrections in the optical model. Proving this would be challenging, as surface measurements during the Q-ALE process are required to understand the cause of the island layer growth. Additionally, other sources, such as native oxide formation during processing, are difficult to exclude, as ellipsometry detects these based on optical parameters. Ultra-sensitive surface elemental analysis tools would be required, as oxygen detection is beyond the resolution of EDS used in this project, necessitating elemental analysis of the ICP-RIE chamber during processing.

Reference GaAs

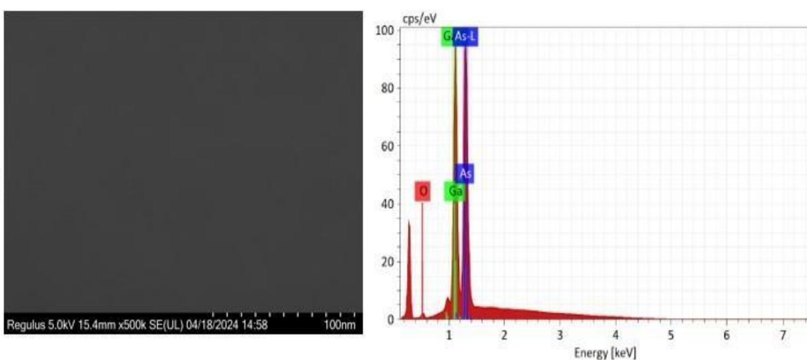

Map

Element	At. No.	Net	Mass [%]	Mass Norm. [%]	Atom [%]	abs. error [mass%] (1 σ)	rel. error [%] (1 σ)
Gallium	31	1188646	46,90	47,74	49,53	1,79	3,83
Arsenic	33	1464156	51,35	52,26	50,47	1,72	3,35
		Sum	98,25	100,00	100,00		

Etched GaAs

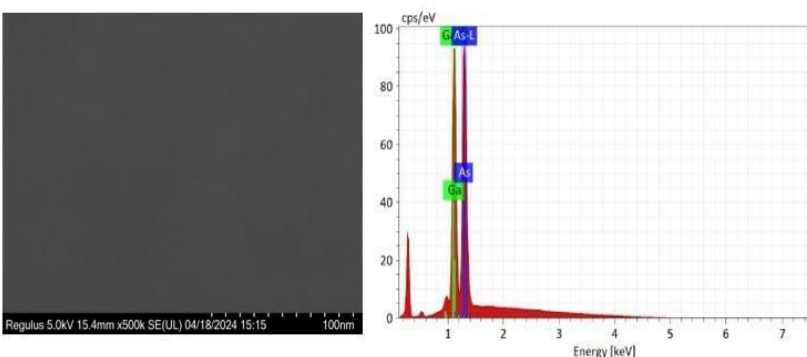

Map

Element	At. No.	Net	Mass [%]	Mass Norm. [%]	Atom [%]	abs. error [mass%] (1 σ)	rel. error [%] (1 σ)
Gallium	31	1076091	46,13	47,71	49,51	1,77	3,84
Arsenic	33	1310598	50,56	52,29	50,49	1,70	3,36
		Sum	96,68	100,00	100,00		

Figure 4.16: SEM images, 5 kV accelerating voltage, MAG 500kX. EDS spectra of reference GaAs and etched GaAs at 60 mTorr according to recipe in Table 3.2 using Si carrier. Neither island formation nor Si are detected on the GaAs surface.

Referance Si

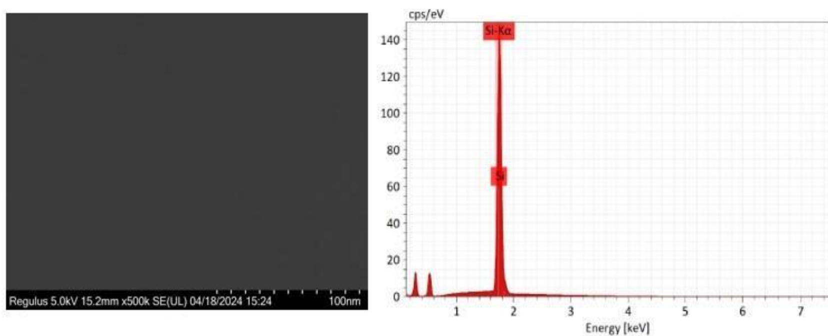

Map

Element	At. No.	Net	Mass [%]	Mass Norm. [%]	Atom [%]	abs. error [mass%] (1 σ)	rel. error [%] (1 σ)
Silicon	14	814371	1,21	100,00	100,00	0,03	2,83
		Sum	1,21	100,00	100,00		

Etched Si

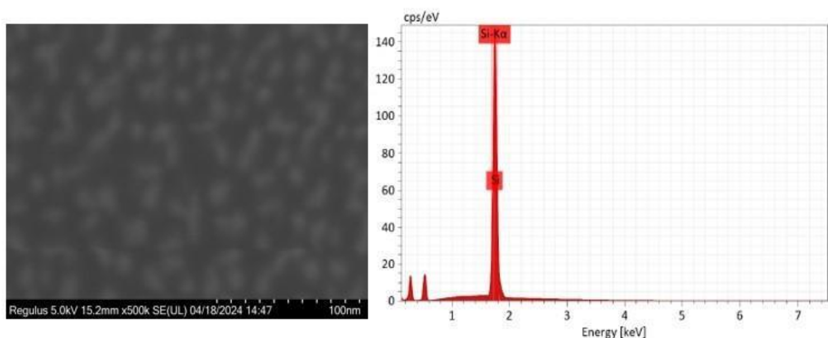

Map

Element	At. No.	Net	Mass [%]	Mass Norm. [%]	Atom [%]	abs. error [mass%] (1 σ)	rel. error [%] (1 σ)
Silicon	14	2062832	158,70	100,00	100,00	5,01	3,16
		Sum	158,70	100,00	100,00		

Figure 4.17: SEM images 5 kV accelerating voltage, MAG 500kX. and EDS spectra of reference Si and etched Si at 60 mTorr according to the recipe in Table 3.2 using Si carrier.

In conclusion, we are dealing with two competing processes: the ALE of Si, the re-deposition of etched/sputtered Si back onto the surface, and surface oxidation. It is highly likely that the re-deposition is responsible for the formation of the surface island formation, which interrupts the etching. However, the impact of surface island formation was not as significant for a lower number of cycles compared to 25 cycles. Therefore, we decided to proceed with the topography evaluation of the samples etched for 25 cycles using AFM, as it is the least affected by this surface island formation.

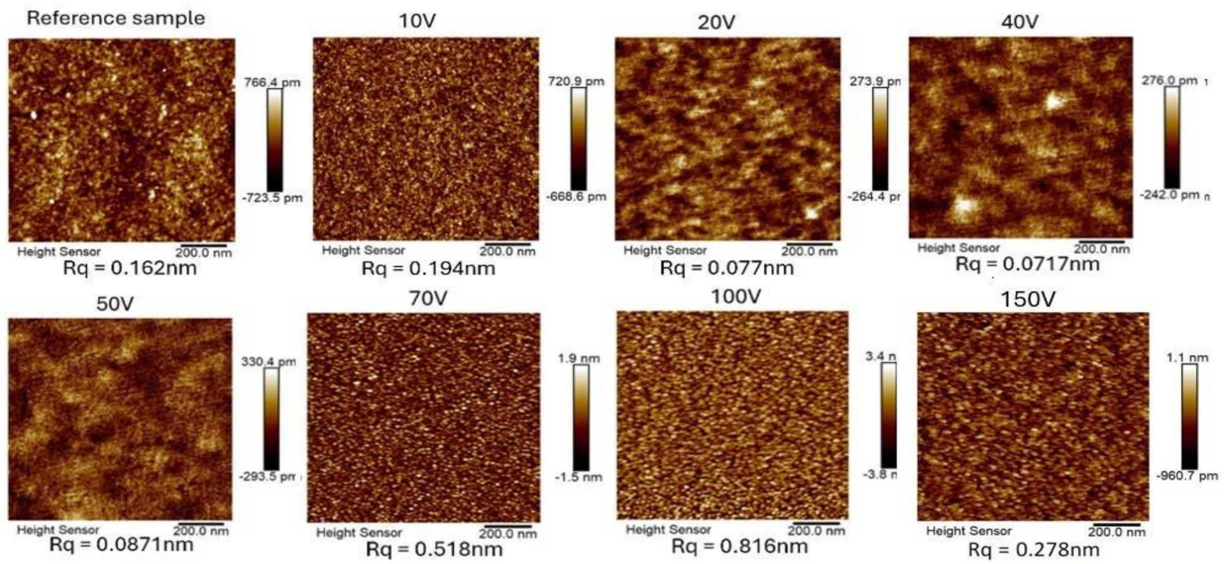

Figure 4.18: AFM images of the etched SOI sample with ALE recipe, Table 4.2, for 10 s etch time and 25 cycles are shown for increasing bias from 10 to 150 V. The figure also shows the root mean square (Rq) of height roughness calculated from the AFM measurement.

Figure 4.18 shows the AFM images of the etched SOI sample using the ALE recipe in Table 4.2, with 10 s etch time and 25 cycles as a function of bias 10 to 150 V. The figure also shows the respective root mean square (Rq) height deviations from AFM measurement to evaluate the surface roughness. In Figure 4.19, the respective values of Rq are plotted versus increasing bias and peak ion energy. Here, one can see that the Rq values are decreasing in the region from 20 V (57 eV peak ion energy) to 50 V (76 eV peak ion energy) to below 0.08 nm in comparison to the reference unetched sample with Rq=0.162 nm. This indicates that the surface roughness is improved for this energy region. This energy region also coincides with what is believed to be the Q-ALE window from Figure 4.8. This means that in the energy region from 20 to 50 V bias, there is a self-limiting etching process, which, at the same time, improves the surface roughness. The improvement of the surface roughness for ALE processing is not something new. It has been described previously in the theoretical background [15], but it indicates that the developed Q-ALE process is within the self-limiting regime of ALE.

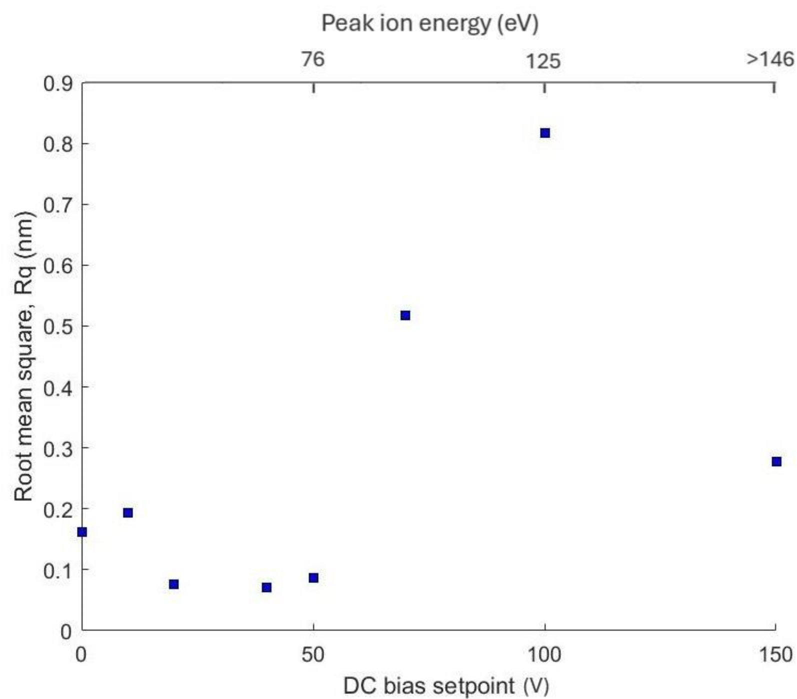

Figure 4.19: Root mean square (Rq) values for AFM measurements in Figure 4.18 plotted versus bias and corresponding peak ion energy from Figure 4.1.

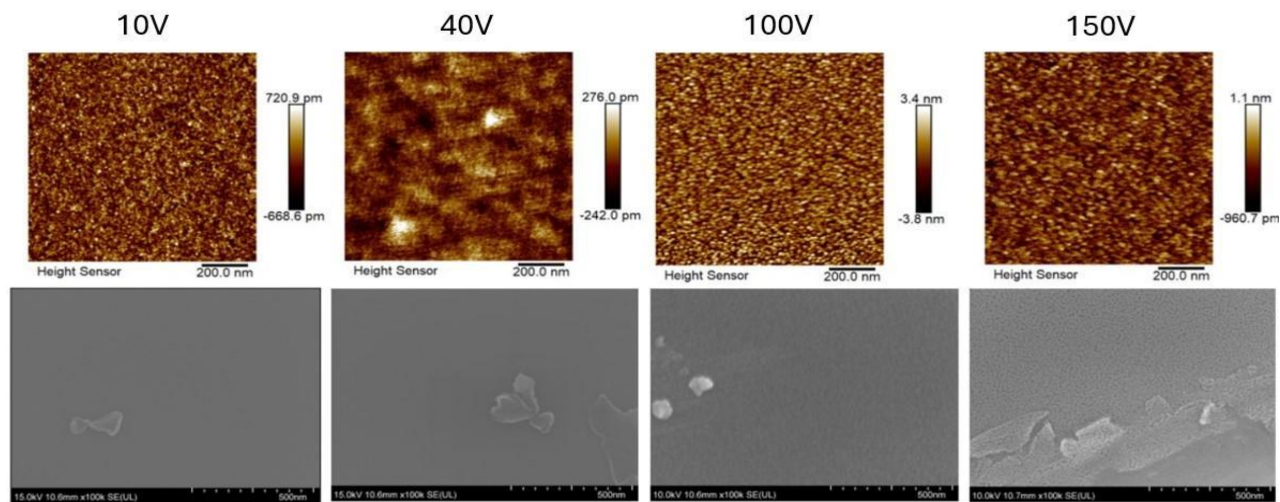

Figure 4.20: AFM measurement with corresponding SEM images 10 kV accelerating voltage, MAG 100kX. SEM Images for samples etched with 10, 40, 100 and 150 V bias.

At the ion energy above 50 V bias, the value of Rq increases, which is expected as higher ion energy will result in more surface roughening and surface damage. However, the increase in Rq reaches its maximum at 100 V bias, corresponding to 125 eV Ar+ ion energy. In Figure 4.20, the respective sample was characterised by SEM, where one can see that the surface of the substrate is affected by the higher bias. For the 150 V bias, the surface was significantly covered by the same island structure as for the increasing number of cycles and coincides with the growth of native oxide according to the ellipsometry optical model. The range of sputtering of Si is expected to lie within the 150 V bias (above 146 eV peak ion energy). Therefore, the surface island formation that has been observed with increasing bias is most likely due to the effect of sputtering. It is highly likely that the high-energy ions, as shown in Figure 4.1, can cause sputtering even at lower bias. Therefore, high-energy ions cannot be ignored, even at low bias. To avoid the effect of sputtering by the Q-ALE process used in this project to achieve the behaviour as for real ALE, the process must be limited to 25 cycles for energies below 100 V bias (125 eV peak ion energy) to reduce the effect of the sputtering effect of high-energy ions.

Chapter 5

Conclusions and further outlook

5.1 Conclusions

The current work is focused on studies of a Q-ALE of Si using Cl_2/Ar chemistry and the corresponding surface effects after etching. Unpatterned silicon-on-insulated samples were used for the etching experiments. The removed Si thickness was measured by spectroscopic ellipsometry, and the etched surface was characterised by SEM and EDS. For the first time, Ar+ ion energy distribution data were obtained and linked to the ALE process and its surface damage. Below are some main conclusions from the study.

- The Ar+ peak ion energy in an RF plasma discharge increases with the DC bias and decreases with pressure. The sputtering threshold for Si should start from 50 to 60 eV, i.e., 7 to 30 V bias, according to RFEA measurements. A low energy peak of around 10 eV was observed for all the measured Ar+ ion energies, likely due to ion collisions at elevated pressure.
- For atomic layer etching (ALE), the 50 to 90eV energy range fits within the self-limiting “ALE window” for silicon, observed at 3 mTorr. Q-ALE experiments show self-limiting behaviour for an EPC just below 1.3Å at 25 to 60V bias (corresponding to 57 to 86 eV peak Ar+ion energy).
- Increasing the time of the etches and the number of cycles at 25 and 40V bias disrupts self-limiting behaviour, decreasing EPC due to the growth of surface islands.
- SEM and EDS analyses reveal island surface deformation from the silicon sample itself, likely due to the redeposition of etched/sputtered Si back to its surface.
- AFM analysis shows improved surface roughness between 25 and 60V bias (corresponding to 57 to 86eV peak ion energy), coinciding with the Q-ALE window. The Q-ALE process should be limited to 25 cycles for energies below 100 V bias (above 125eV peak ion energy) to avoid sputtering and redeposition effects.

5.2 Further outlook

- Continue with more research using in-situ plasma characterisation tools for a better understanding of ICP-RIE plasma conditions with reduced IEDF broadening and better control over ion state in the Q-ALE.
  process.

- Explore the effects of using both ICP and RF as power sources, as ICP is known to have narrower ion energy distribution and more dense plasma.

- Optimize the Q-ALE process parameters to achieve self-limiting behaviour similar to real ALE by increasing etch time and cycles to minimize surface island formation and damage, making Q-ALE beneficial for semiconductor applications.

- Investigate Q-ALE with different materials since that GaAs do not show surface island formation like Si. Explore if other III-V materials exhibit similar behaviour with Q-ALE, as a self-limiting etching process improving surface roughness would be valuable for the semiconductor industry.

- Use Kelvin probe force microscopy (KPFM) to analyse surface potential variations and gain insights into surface chemical states and work function changes. This can help optimize the Q-ALE process, reducing surface damage and improving etching uniformity.

Bibliography

[1] Kanarik K J Lee C G N and Gottscho R A. The grand challenges of plasma etching: a manufacturing perspective. DOI: 10.1088/0022-3727/47/27/273001, June 2014. (HÄMTAD 10/31/2023).

[2] Tan S Kanarik K J and Gottscho R A. Atomic layer etching: Rethinking the art of etch. J. Phys. Chem. Lett. 2018, 9, (4814–4821). DOI: 10.1021/acs.jpclett.8b00997J, August 2018. (HÄMTAD 10/31/2023).

[3] Isobe M Tinacba E J C and Hamaguchi S. Surface damage formation during atomic layer etching of silicon with chlorine adsorption. https://doi.org/10.1116/6.0001117, June 2021. (HÄMTAD 10/31/2023).

[4] David Humbird Joseph R. Vella and David B. Graves. A molecular dynamics study of silicon atomic layer etching by chlorine gas and argon ions. Princeton Plasma Physics Laboratory, Princeton, NJ 08540 USA, J. Vac. Sci. Technol. B 40, 023205 (2022), (1-8), https://doi.org/10.1116/6.0001681, February 2022. (HÄMTAD 8/21/2023).

[5] Alabrash M. Damage analysis of reactive ion and atomic layer etched silicon. (15-18) http://lup.lub.lu.se/student-papers/record/9123831, May 2023. (HÄMTAD 10/31/2023).

[6] Z. Cui. Nanofabrication. Cham: Springer International Publishing AG, (240-249), 2008. (HÄMTAD 09/15/2023).

[7] Peizhi Wang and Fengzhou Fang. Defect-mediated atomic layer etching processes on cl–si(100): An atomistic insight. https://doi.org/10.1021/acs.jpcc.3c05378. (HÄMTAD 11/07/2023).

[8] Uros Cvelbar Petr Spatenka K.M. Praveen Sabu Thomas Miran Mozetic Uros Cvelbar Petr Spatenka K.M. Praveen Sabu Thomas, Miran Mozetic. Non-thermal plasma technology for polymeric materials, Elsevier Science, (23-65). doi.org/10.1016/C2016-0-03254-0, October 2018. (HÄMTAD 10/31/2023) .

[9] A. Godines R. Asomoza Y. Kudriavtsev, A. Villegas. Calculation of the surface binding energy for ion sputtered particles. https://doi.org/10.1016/j.apsusc.2004.06.014, January 2005. (HÄMTAD 8/21/2023).

[10] Fengzhou Fang Peizhi Wang a, Marco Castelli a. Mechanism of photo-assisted atomic layer etching of chlorinated si(111) surfaces: Insights from DFT/TDDFT calculations. https://doi.org/10.1016/j.mssp.2022.107169, January 2023. (HÄMTAD 10/31/2023)

[11] E.A. Hudson S. Sriraman S. Tan J. Marks V. Vahedi R.A. Gottscho K.J. Kanarik, T. Lill. ”overview of atomic layer etching in the semiconductor industry. J. Vac. Sci. Technol. A 33, 020802, 1–13) https://doi.org/10.1116/1.4913379, March 2015. (HÄMTAD 8/21/2023).

[12] Ekaterina N. Voronina Alexander P. Palov, Gabriel G. Balint-Kurti and Tatyana V. Rakhimova. Sputtering of si by ar: A binary collision approach based on quantum-mechanical cross sections. J. Vac. Sci. Technol. A 36, 041303, (1 –9) https://doi.org/10. 1116/1.5027387, 2018. (HÄMTAD 8/21/2023).

[13] Erin Joy Capdos Tinacba ; Michiro Isobe; Satoshi Hamaguchi. Surface damage formation during atomic layer etching of silicon with chlorine adsorption. J. Vac. Sci. Technol. A 39, 042603, Issue 4 (1–9) https://doi.org/10.1116/6.0001117, 2021. (HÄMTAD 8/21/2023).

[14] Bernd Rauschenbach. Low-energy ion irradiation of materials. SSMATERIALS, volume 324. Springer (9-122) Book, August 2022. (HÄMTAD 02/01/2024).

[15] Sven H. Gerritsen Nicholas J. Chittock* Vincent, Vandalon Marcel A. Verheijen Harm C. M. Knoops Wilhelmus M. M. Kessels Sven H. Gerritsen Sven H. Gerritsen Department of Applied Physics, Eindhoven University of Technology and Adriaan J. M. Mackus*. Surface smoothing by atomic layer deposition and etching for the fabrication of nanodevices. ACS Appl. Nano Mater. 2022, 5, 18116−18126 https://doi.org/10.1021/acsanm.2c04025, November 2022. (HÄMTAD 08/28/2023).

[16] Oxford instruments. Atomic layer etching (ale). https://plasma.oxinst.com/technology/atomic-layer-etching, (HÄMTAD 01/22/2024).

[17] Peng Zhang Bingjun Yu Cheng Chen Tianbao Ma Xinchun Lu Seong H. Kim Lei Chen, Jialin Wen and Linmao Qianc. Nanomanufacturing of silicon surface with a single atomic layer precision via mechanochemical reactions. *Nature Communications* volume 9,Article number: 1542.(1-5)[DOI:10.1038/s41467-018-03930-5].(HÄMTAD 11/06/2023).

[18] D. Metzler G. S. Oehrlein and C. Li1. Atomic layer etching at the tipping point: An overview. ECS Journal of Solid State Science and Technology 4, (N5041-N5051), [DOI: 10.1149/2.0061506jss], 2015 (HÄMTAD 11/06/2023).

[19] Thorsten Lill. Atomic layer processing. Wiley-VCH; 1st edition (7-42), April 2021. (HÄMTAD 8/18/2023).

[20] M. Nakamur D. Metzler S. G. Walton S. U. Engelmann, R. L. Bruce and E. A. Joseph. Challenges of tailoring surface chemistry and plasma/surface interactions to advance atomic layer etching. [DOI: 10.1149/2.0101506jss], April 2015. (HÄMTAD 01/24/2024).

[21] Yoana Ilarionova. Real- and Quasi-atomic layer etching for ultra-high resolution patterning. http://lup.lub.lu.se/student-papers/record/9105925, 2022. (HÄMTAD 07/11/2023).

[22] Ivan L. Berry; Keren J. Kanarik; Thorsten Lill; Samantha Tan; Vahid Vahedi; Richard A. Gottscho. Applying sputtering theory to directional atomic layer etching. *J. Vac. Sci. Technol. A* 36, 01B105 (2018), (1-8) https://doi.org/10.1116/1.5003393. 2017 (HÄMTAD 07/11/2023).

[23] *R.Entner: Modeling and Simulation of Negative Bias Temperature Instability, https://www.iue.tuwien.ac.at/phd/entner/node14.html, April 2007. (HÄMTAD 04/04/2024).*

[24] Akiko Hirata. Reduction of process-induced damage in atomic layer etching. Sony Semiconductor Solutions Corporation, IEEE, February 2021. (HÄMTAD 04/04/2024).

[25] Zheng Cui. Nanofabrication principles, capabilities and limits. Cham: Springer International Publishing AG, (238-240) Book, 2008. (HÄMTAD 05/04/2024).

[26] Dominik Metzler. Investigation of thin oxide layer removal from si substrates using an sio2 atomic layer etching approach: the importance of the reactivity of the substrate. *et al* 2017 *J. Phys. D: Appl. Phys.* **50** 254006 https://doi.org/10.1088/1361-6463/aa71f1, June 2017. (HÄMTAD 04/04/2024).

[27] Plasma-Therm LLC. Takachi icp .http://www.plasmatherm.com/Takachi_ICP.html. (HÄMTAD 8/30/2023).

[28] Plasma-Therm. Plasma etching:comparing pe, rie and icp-rie. https://corial.plasmatherm.com/ whitepaper-plasma-etching-comparing-pe-rie-and-icp-rie, October 2020. (HÄMTAD 8/30/2023).

[29] David,G,Lishan.Plasma etching-comparing pe, rie and icp-rie.https://www.researchgate.net/publication/347595123_Plasma_Etching_Comparing_PE_RIE_and_ICP-RIE, October 2020. (HÄMTAD 8/30/2023).

[30] Impedans. Semion rfea system measure the ion flux and ion energy incident on your substrate. https://www.impedans.com/wp-content/uploads/2021/12/Semion-Technical-Presentation.pdf,January.(HÄMTAD 04/15/2024).

[31] Impedans plasma measurments. Semion single / multi system, installation user guide. Installation and User Guide, November. (HÄMTAD 04/15/2024).

[32] Hiroyuki Fujiwara. Spectroscopic ellipsometry: Principles and applications. ISBN:9780470060193, Januari 2007. (HÄMTAD 8/31/2023).

[33] Blomqvist. Peter. Ellipsometry - guidelines and tips. https://lundnanolab.ftf.lth.se/display/FP/User+Manuals+-+Woollam+RC2?preview=/25100410/40861738/PBL_Ellipsometry_Tutorial%20-%20Measurement.pdf, Mars 2021. (HÄMTAD 08/25/2023).

[34] BRUKER.Spectroscopic ellipsometry. https://www.bruker.com/en/products-and-solutions/test-and-measurement/ellipsometers-and-reflectometers/spectroscopic-ellipsometers.html. (HÄMTAD 08/25/2023).

[35] James N. Hilfiker Blaine Johs Dhananjay I. Patel, Dhruv. Shah. A tutorial on spectroscopic ellipsometry (se), 3. Surface-roughness.https://www.researchgate.net/publication/333247678_A_Tutorial_on_Spectroscopic_Ellipsometry_SE_3_Surface_Roughness, June 2019. (HÄMTAD 23/11/2023).

[36] John T. Thornton Phil Russel. Sem and AFM: Complementary techniques for high-resolution surface investigations.chrome-extension://efaidnbmnnnibpcajpcglclefindmkaj/https://www.bruker-nano.jp/library/57e489500c201abd043451c7/57fde5b1c686f9d96b44b14c.pdf. (HÄMTAD 21/03/2024).

[37] Bruker Nano GmbH. Quantax flatquad eds for sem with the xflash® flatquad. https://www.bruker.com/en/products-and-solutions/elemental-analysers/eds-wds-ebsd-SEM-Micro-XRF/quantax-flatquad. html. (HÄMTAD 04/17/2023).

[38] C. Barry Carte David B.Williams. Transmission electron microscopy Diffraction, Imaging, and spectrometry. Springer International Publishing AG. (19-65) September 2016 (HÄMTAD 04/17/2023).

[39] DALE E. NEWBURY. Mistakes encountered during automatic peak identification in low beam energy x-ray microanalysis. Scanning VOL. 29(4),(137-151), https://doi.org/10.1002/sca.20009 , 2007. (HÄMTAD 04/04/2024).

[40] KTH.Atomicforcemicroscopy(afm).https://www.nanophys.kth.se/nanolab/afm/icon/bruker-help/Content/SPM%20Training%20Guide/Atomic%20Force%20Microscopy%20(AFM)/Atomic%20Force%20Microscopy%20(AFM).htm. (HÄMTAD 08/28/2023).

[41] Eaton, Peter, and Paul West, *Atomic Force Microscopy* (Oxford, 2010; online edn, Oxford Academic, 1 May 2010), https://doi.org/10.1093/acprof:oso/9780199570454.001.0001. May 2010. (HÄMTAD 08/28/2023).

[42] Plasma-Therm LLC. Takachi icp. http://www.plasmatherm.com/Takachi_ICP.html. (HÄMTAD 21/03/2024).

[43] D. Andruczyka T. Choa D.N. Ruzic*a S. N. Srivastavab J. Sporrea, D. Elga and D.C. Brandtb. In-situ sn contamination removal by hydrogen plasma. Extreme Ultraviolet (EUV) Lithography III, Volume 8322 (Proceedings of SPIE - The International Society for Optical Engineering; Vol. 8322), DOI:10.1117/12.916434, March 2012. (HÄMTAD 21/03/2024).

[44] Jeol.Energy table for eds analysis. https://www.unamur.be/services/microscopie/sme-documents/Energy-20table-20for-20EDS-20analysis-1.pdf. (HÄMTAD 04/25/2023).